Co-Optima Final Report

Federal Agency & Organization: Department of Energy – Bioenergy Technologies Office
Project Title: Rapid Construction of Validated Chemistry Models for Advanced Biofuels
Award Number: DE-EE0007982

Recipient Organization: MIT
Principal Investigator: William H. Green
Project Location: 02139

Reporting Period: Jan 15, 2017 to Dec 31, 2020
Date of Report: Oct 15, 2021

Acknowledgment: This material is based upon work supported by the U.S. Department of Energy's Office of Energy Efficiency and Renewable Energy (EERE) under the Bioenergy Technologies Office Award Number DE-EE0007982.

Table of Contents

Abstract/Executive Summary

Computer methods were developed and demonstrated that make it possible to predict the combustion and pyrolysis chemistry of proposed biofuels, even before the biofuels are ever manufactured or experimentally tested. The methods are based on first-principles calculations of reaction rates and equilibria. A large number of complicated calculations are required, so we developed a computer workflow that automates many of the steps. With the chemical structure of the biofuel and the system conditions (temperature, pressure, compositions, etc.) as the input, the computer methods can construct a detailed kinetic model with refined parameters without intense human intervention. The automation of model construction makes it practical for a single engineer to make the predictions in a reasonable time period. The accuracy of the computer predictions was tested by measuring the time-profiles of various reaction intermediates (carbon monoxide, carbon dioxide, water, formaldehyde, methane, and ethylene) formed as the biofuels pyrolyze or ignite using sophisticated laser shock tube methods. Several biofuels, including methyl propyl ether, cyclopentanone, butyl acetate isomers, etc., were carefully studied to demonstrate the validity of the proposed computational and experimental methodology. This research project opens up the possibility for assessing some proposed biofuels on the computer without expensive experimental campaigns. The new computer methods are open source and well-documented, allowing a knowledgeable modeler to easily access the developed methods and implement them in their work routine. Moreover, they are also convenient and powerful, promising for developing the fuel chemistry models needed for use in engine simulators, facilitating co-optimization of new engine designs with new fuels.

Background

Dozens of potential biofuels are under consideration for use in future engines. It is impractically difficult and expensive to experimentally test each potential biofuel in each proposed future engine at all engine conditions, so there is great interest in using computer models to reduce the number of experiments required and to help guide and interpret the experiments. These computer models are also very helpful for co-optimizing the engine to match the fuel.

At the time this project began, there were indications that it might be possible to use a computer to construct the combustion chemistry models for new biofuels, including to compute all the reaction rates and thermochemical parameters involved, using quantum chemistry, rate theory, and automated mechanism generation software such as the Reaction Mechanism Generator (RMG) package.[1] However, the then-existing process for constructing combustion chemistry models was quite slow and tedious (e.g., it had taken four years for a large team of investigators to build and test a combustion chemistry model for isobutanol, a rather simple biofuel[2]), and the methods for experimentally validating such models were also not completely satisfactory.

This project's goal was therefore to develop a much more efficient computational workflow for building the combustion chemistry models for biofuels, making it practical for a single chemist or chemical engineer to construct accurate models for several relatively complicated biofuels each year, rather than a single very simple biofuel taking multiple years. Similarly, this project aimed to demonstrate how the models could be experimentally validated about as fast as they were created. Both goals required developing improved methods and efficient workflows. In some cases, these were straightforward improvements on existing methods (e.g., improvements to the RMG and ARKANE software packages, and development of low-pressure optical probes for HCHO). In other cases, completely new software needed to be developed (e.g., the new ARC package developed during this project), and some new experimental probes also had to be developed.

Chapter 1 Selection of Target Biofuels

The selection of target biofuels was made according to our discussion with our LLNL mentor, William J. Pitz, and other national lab and university members of the Co-Optima team about which fuels were most in need of chemical kinetic models. In total, ten biofuel molecules are selected:

1. Methyl propyl ether: high production maturity, high cetane number, good example for understanding combustion chemistry of ethers.
2. Cyclopentanone: Tier 3 biofuel. High energy density, high research octane number (RON) and sensitivity enhancement, low soot formation tendency.
3. n-butyl acetate: Tier 2 biofuel. Potential biodiesel additive.
4. i-butyl acetate: same as n-butyl acetate.
5. s-butyl acetate: same as n-butyl acetate.
6. t-butyl acetate: same as n-butyl acetate.
7. 3,3-dimethylpent-1-ene: A biofuel exhibits high phi sensitivity.
8. 3,4-dimethylpent-1-ene: A biofuel exhibits high phi sensitivity.
9. 1-octene: A biofuel exhibits high phi-sensitivity.
10. 2,3-dimethylbut-2-ene: A biofuel exhibits hyper-boosting effect.

The corresponding structures of each biofuel molecule are shown in Figure 1.

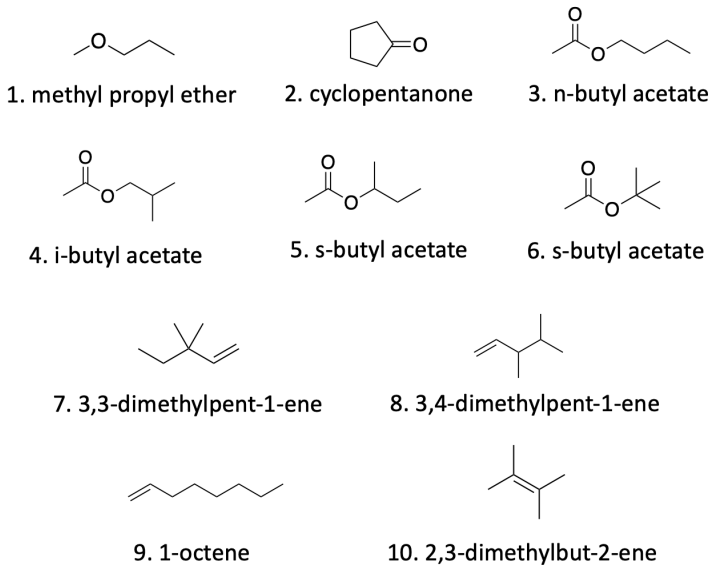

Figure 1. *The corresponding structures of each biofuel molecule.*

The first two biofuels were modeled in the first year of the project, and their models are also called Y1 models; the third to the sixth were modeled in the second year of the project (Y2 models); the last four biofuels were modeled in the third year of the project (Y3 models).

Chapter 2 Carbon Monoxide Diagnostic Scheme Developed, Demonstrated, and Applied to Target Biofuels

Carbon monoxide is one of the key combustion intermediates, and its time histories can be used to validate and test the kinetic model of a biofuel. The current state-of-the-art is that such time histories are usually measured at P < 10 atm, and we used this known technology to measure CO formation from several proposed biofuels, testing combustion models, see section 2.1. At higher pressure quantifying the CO using spectra becomes more complicated, and absorption signals smaller, due to pressure-broadening effects. We performed extra spectroscopy experiments that allowed us to correctly quantify CO concentrations at high pressure. One application of this new high-pressure probe technique is shown in Section 2.2. Enlarging the measured pressure range to 30 atm allows validating models in the conditions of interest (e.g., conditions relevant to the compression-ignition engine) and thus further improves the confidence of predictions from model simulations. It is also true for HCHO (discussed in Chapter 3) and other combustion intermediates (discussed in Chapter 6).

2.1 Measure CO Time Histories for Pressures up to 10 atm

Diagnostics to measure carbon monoxide time-histories in a shock tube were developed and optimized for pressures up to 10 atm. A distributed feedback quantum cascade laser from Alpes Lasers (TO3-L-50) was utilized for these measurements. Initial CO measurements were made during the oxidation of cyclopentanone in a collaborative effort with LLNL (Figure 2). In this work[3], CO time-histories were measured over a large temperature span (1100-1500 K) at pressures of 1, 6, and 8.5 atm. In this initial study, absorption cross-sections for CO were taken from the HITRAN 2012 database[4]. Measured CO time-histories and ignition delay times were in good agreement with the developed mechanism by our collaborators.

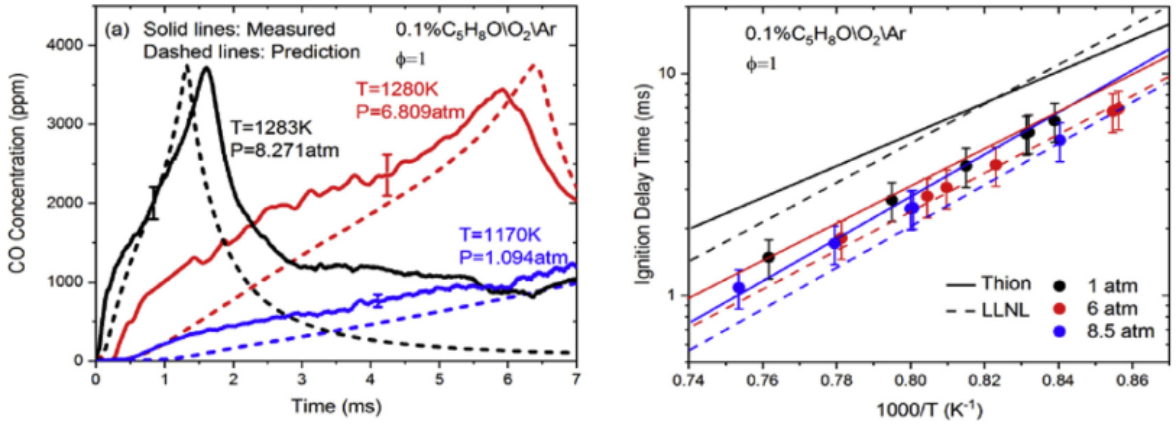

Figure 2. *CO time-history data during cyclopentanone oxidation. (a) Examples of experimental and simulated CO time-histories, solid lines are experimental results and dashed are simulations from Zhang et al.[3]; (b) experimental and simulated ignition delay times at phi=1 and P=1, 6, and 8.5 atm, solid symbols are experiments and solid and dashed lines are linear fits of simulations by Thion et al.[6] and Zhang et al.[3], respectively. Data published as part of Co-Optima project by Zhang et al.[3]*

In measurements of CO, we measured the molecules' absorption cross-section near 10 atm over the temperatures 1085-1456 K inside our shock tube apparatus. The equation governing carbon monoxide's absorption cross-section at these conditions and 2046.30 cm^{-1} is provided in one of

our publications on this effort by Ninnemann et al.[5] Using this empirical relation, we measured CO time-histories up to 10 atm on diisobutylene oxidation (Figure 3), propyl methyl ether oxidation and pyrolysis (Figure 4), 1 and 2-pentene oxidation (Figure 5), and prenol and isoprenol oxidation (Figure 6).

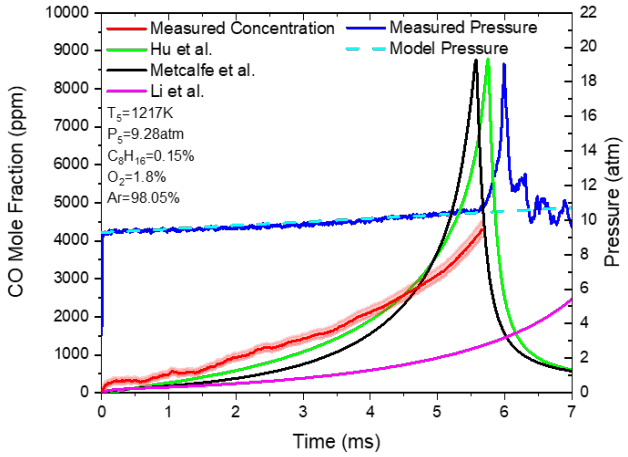

Figure 3. *CO time-history data during diisobutylene oxidation. Red line is measured CO mole fraction and blue is measured pressure. Black[7], green[8] and magenta[9] lines are simulated CO time-histories from recent literature mechanisms.*

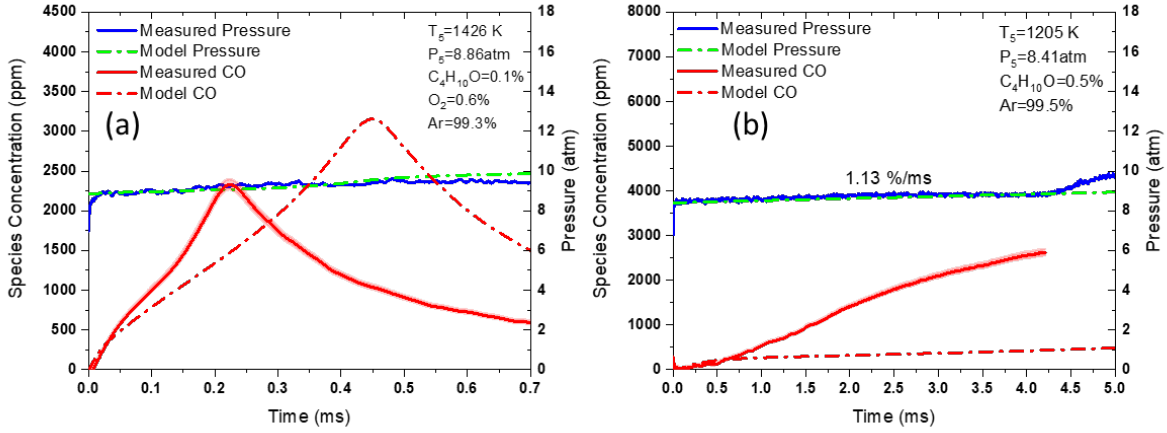

Figure 4. *CO time-history during propyl methyl ether (a) oxidation and (b) pyrolysis. Solid red and blue lines are experimental CO time-histories and pressure, respectively. Dashed red and green lines are the simulated CO time histories and model pressure input, respectively. Mechanism used is the propyl methyl ether mechanism developed by the Green group at MIT[10].*

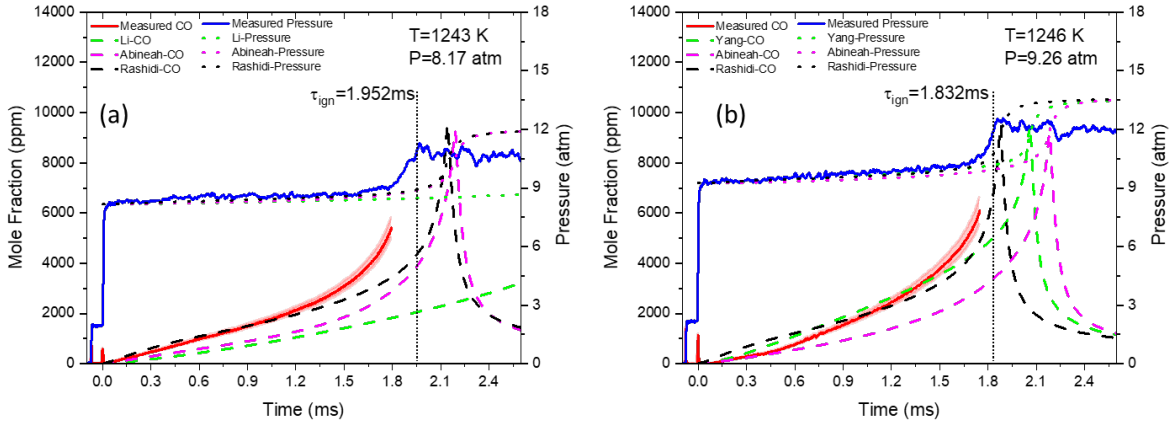

Figure 5. *CO time-histories for the oxidation of 0.25%fuel/1.87%O_2/Ar for the isomers (a)trans-1-pentene and (b) trans-2-pentene. Solid red and blue lines are experimental CO time-histories and pressure, respectively. Dashed lines are simulated CO time-histories using the mechanisms of Li et al.*[11] *(green), Abineah et al.*[12] *(magenta), and Rashidi et al.*[13] *(black).*

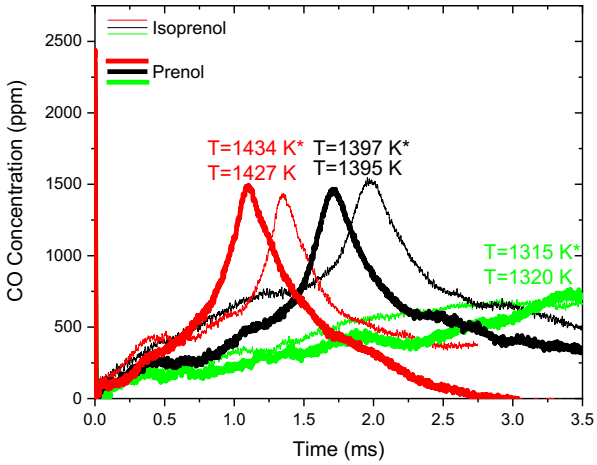

Figure 6. *CO time histories as a function of temperature for the isomers prenol and isoprenol. Mixtures were 0.05% fuel/0.35%O_2/Ar, pressures were about 9 atm. Data published as part of the Co-Optima project by Ninnemann et al.*[5]

2.2 Measure CO vs. Time for High P

Shock tube measurements were conducted for several conditions of ethanol oxidation near 20 atm. Temperatures spanned 960-1580 K, equivalence ratios were varied from 0.5 to 1.0, and the fuel loading was varied from 0.25-6.54%. For these measurements, the absorption cross-section of carbon monoxide was measured at 20 atm over the experimental temperature range[14] and used to infer CO concentrations during ethanol oxidation. Results are provided in Figure 7.

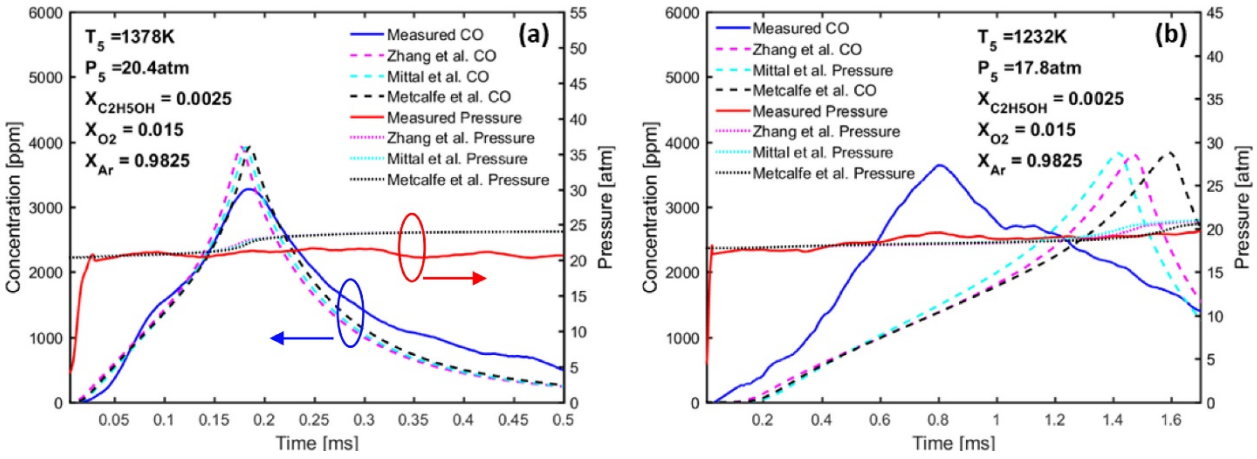

Figure 7. *High pressure CO time-histories for ethanol oxidation at (a) 1378 K and 20.4 atm and (b) 1232 K and 17.8 atm. Solid red and blue lines are experimental pressure and CO time-histories, respectively. Dashed lines are simulated CO time-histories using the mechanisms of Zhang et al.*[15] *(magenta), Metcalfe et al.*[16] *(black), and Mittal et al.*[17] *(teal). This data was published as part of the Co-Optima project by Laich et al.*[14]

Chapter 3 Measure HCHO Time Traces

Formaldehyde (HCHO) is an important combustion intermediate, nearly as ubiquitous as CO but even more important for the ignition chemistry. We developed a high-accuracy laser probe technique for HCHO for P<10 atm and made a few measurements of HCHO time profiles relevant to biofuel chemistry, see section 3.1. Unfortunately, the laser then died, and before it could be replaced the pandemic shuttered our laboratories, so we were not able to perform as many HCHO measurements as initially contemplated.

3.1 HCHO Measurements at Low P

Diagnostics for HCHO measurements in a shock tube were configured and optimized for low pressures. A distributed feedback quantum cascade laser from mirSense (uniMIR-1745-DFB-CW) outputting at 1745cm^{-1} was used. As with the carbon monoxide measurements, the absorption cross-section of HCHO was measured in-house rather than relying on the HITRAN database[4]. Our measurements used trioxane, a trimer of formaldehyde, as the source of anhydrous aldehyde. A comparison between the measured cross-sections using this laser and 0.2% trioxane/Argon mixture and values from the HITRAN database are shown in Figure 8. Using this experimental data for the absorption cross-section, HCHO time-histories were obtained during the pyrolysis of 0.75% propyl methyl ether in argon (Figure 9).

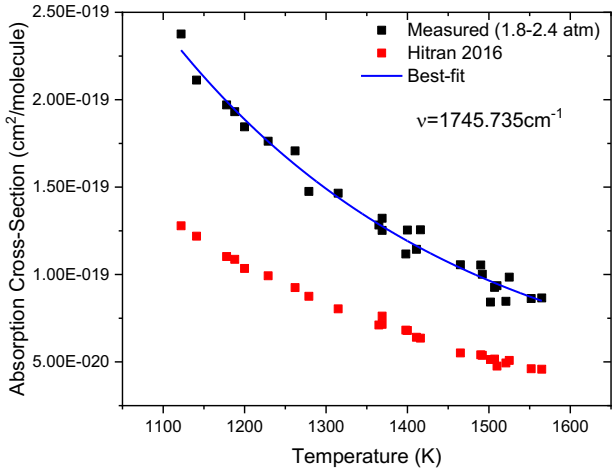

Figure 8. *Experimental HCHO absorption cross-section at 1745.735 cm^{-1} and 1.8-2.4 atm compared to that of the HITRAN database[4]. Mixtures were 0.2% trioxane in Argon. Trioxane is a trimer of formaldehyde such that formaldehyde concentrations behind the reflected shockwave were 3x that of the initial trioxane concentration.*

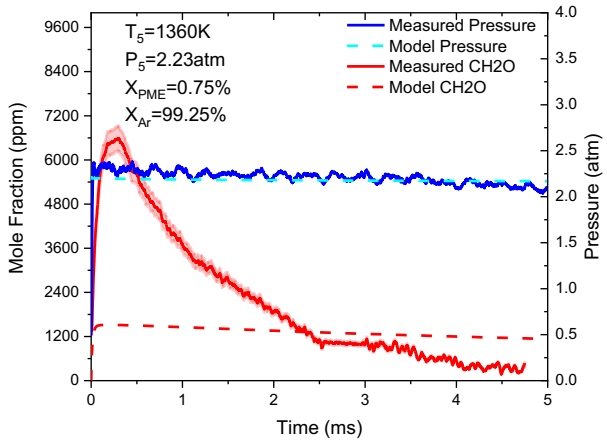

Figure 9. *Experimental HCHO (solid red lines) and pressure trace (solid blue line) during the pyrolysis of 0.75% methyl propyl ether. Dashed red line is generated from the propyl methyl ether mechanism developed by the Green group at MIT*[10]*.*

3.2 HCHO Measurements at High P

Unfortunately, not long after these measurements were made, the laser used for the measurements stopped lasing and future measurements were heavily delayed. The same manufacturer could not supply a QCL with the same output wavelength as previously acquired and eventually another QCL from Alpes lasers (sbcw9394), outputting at 1740 cm^{-1}, was sourced. Experiments using this new laser were planned to measure HCHO concentrations during methyl propyl ether pyrolysis up to 10 atm but were delayed due to COVID-19. Additional measurements were never performed.

Chapter 4 Construct and Refine Kinetic Models

The main objective of this project was to construct accurate combustion chemistry models for several biofuels. To do that, we needed to develop a new/improved workflow. In this chapter we first explain the improvements to the workflow (Section 4.1) and then present the new models for several fuels, with some experimental validations (Sections 4.2, 4.3, 4.4). This chapter is just a summary of what we did; for full technical details, see our journal articles, the software we developed, and the databases which are available online.

4.1 General Methodology and Improvements in the Workflow

The original model construction and refinement process is illustrated in Figure 10. In each iteration, a model was generated for the conditions of interest using the open source RMG software package[1] (mostly developed and maintained by the team at MIT) with the chemical knowledge stored in RMG's database or from calculations done this study. RMG was significantly enhanced during this project in order to make it capable of accurately predicting the combustion chemistry of new biofuels, and of fitting into the complete workflow shown in Figure 10. This initial model was compared against experimental data, and then sensitivities to all rate coefficients and Gibbs free energies of formation were calculated for key observable species concentrations to identify the sensitive species thermochemistry and sensitive reaction rate coefficients. Sensitive parameters were then computed quantum mechanically (using commercially available software, e.g., Gaussian, combined with Arkane, another software package developed by the team at MIT) or extracted from literature for the use in the next iteration. At the time this project began and throughout Year 1, all the steps shown in gray in Figure 10 were performed one-by-one supervised by a human, making the iterative loop quite slow and tedious.

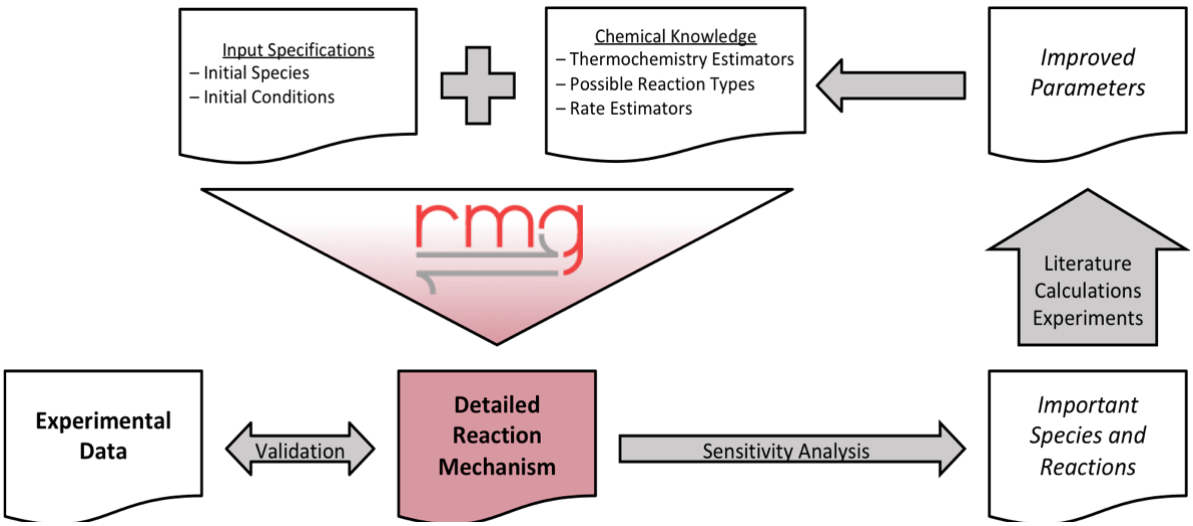

Figure 10. *Original RMG centered model generation workflow.*

While keeping the skeleton of the original RMG's model generation workflow, the workflow's major improvements during this project consist of three aspects, (1) automated quantum chemistry and statistical mechanics calculations, Section 4.1.1 (2) machine learning rate estimator, Section 4.1.2, and (3) improved thermochemical estimation for species with intramolecular hydrogen bonds, Section 4.1.3. These improvements involve adding new features to the code of RMG and Arkane,

additions to the RMG database, and also the development of a new software package called the Automatic Rate Calculator (ARC).

4.1.1 Automated Parameter Calculation

Improving parameters is one of the major bottlenecks of the original workflow. As shown in Figure 11, even to calculate a single parameter, researchers have to know cheminformatics, quantum mechanics, chemical kinetics, statistical mechanics, and supercomputer operation, and they need to finish multiple tasks and interact with different software to perform calculations. Very few researchers are experts in all of these subfields, and even for such experts it is very time-consuming to compute all the parameters relevant to a single reaction. But in this project, to create accurate models for ten proposed biofuels, we need parameters for more than a thousand chemical species and a similarly large number of reactions. Clearly a different, more efficient, workflow is needed to make it practical to do the computations. A new software package, the Automatic Rate Calculator (ARC), an open-source software used to coordinate and manage quantum chemistry and statistical mechanics calculations automatically, was initiated (since the second project year), improved, and applied to automate parameter calculation. An example workflow used by ARC is shown in Figure 12.

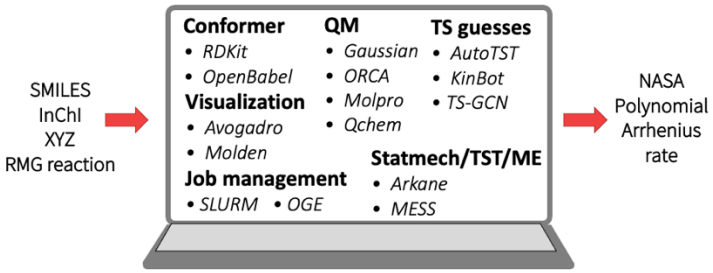

Figure 11. *An illustration of tasks and packages to deal with during the step of improving parameters.*

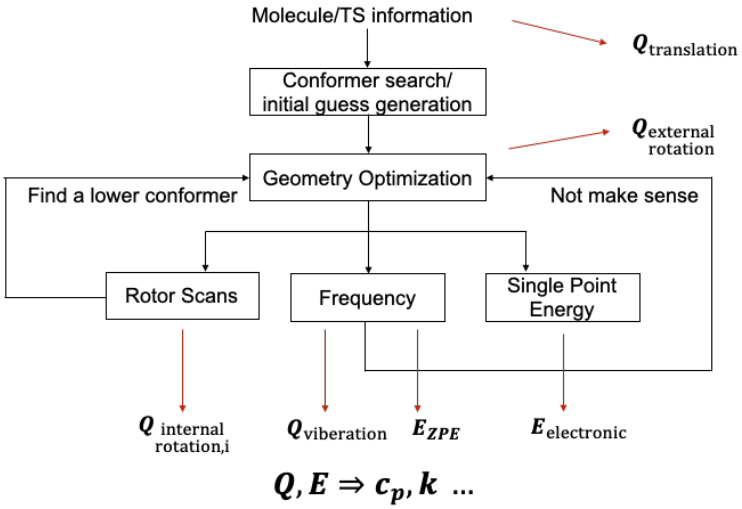

Figure 12. *A workflow for thermochemical data and rate coefficients calculation used by ARC.*

A major effort was put on refining the hindered-rotor-related calculation module, which was the key to get accurate thermodynamic properties and rate coefficients at combustion or pyrolysis temperature. Several key scientific questions and practical issues were discussed and solved. ARC can now detect internal coordinate changes, find the lowest conformer along the rotor scan path, propose solutions to problems, and automatically relaunch required calculations for correction. Besides improvement in the rotor-related calculation module, we also improved periphery modules (e.g., server communication module) to allow workflows being more strictly followed and more robustly conducted.

Besides, the use of ARC enabled us to update correction factors, such as frequency scaling factor and bond additivity correction factors, more easily. For instance, ARC was used to calculate the atom correction and bond additivity correction values for CCSD(T)/def2-tzvp//wb97xd/def2tzvp level of theory that is useful for calculating H atom addition reactions.

Generally speaking, a significant improvement in calculation efficiency was achieved. As an example, at the time of developing the cyclopentanone model, when ARC was not available, we only had sufficient manpower to perform quantum calculations for tens of species. But since then, we have made the workflow orders of magnitude more efficient: more than a thousand species' thermochemical data has been calculated during the last 2 years.

4.1.2 Subgraph Isomorphic Decision Tree Rate Estimator

While ARC significantly reduced the cost of updating parameters, an algorithm for generating subgraph isomorphic decision trees for rate estimation was developed for more efficient use of data and implemented in the code of RMG. This work was selected into Co-Optima FY19 Highlights, and details about this algorithm are included in an in-preparation publication.

The algorithm essentially associates differences in rate estimation with differences in sub-structures on the reactant or reactants. The tree splits reactions into groups with similar rates by identifying the substructural differences that affect rate estimation the most, as shown in Figure 13. The schematic diagram of the training algorithm is given in Figure 14. A set of possible substructures is generated, and the substructure that results in a split that reduces the prediction uncertainty the most is chosen and added to the tree. Once the tree is generated, the kinetics for the reactions matching each node are fit to a Blower-Masel estimator[18] (an improved version of Evans-Polanyi estimator[19]) that accounts for differences in heat of reaction. Rates can then be estimated by descending a reaction down the tree to identify the most specific node it matches and using the Blower-Masel interpolant at this node to estimate the rate coefficient.

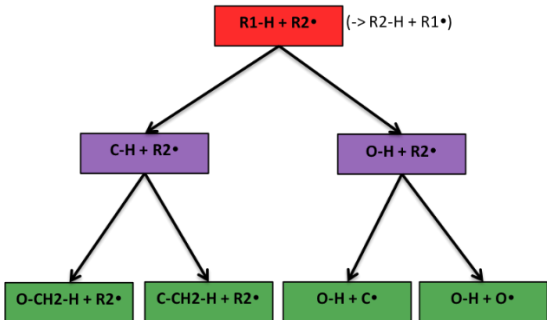

Figure 13. *Subgraph isomorphic reaction template decision tree.*

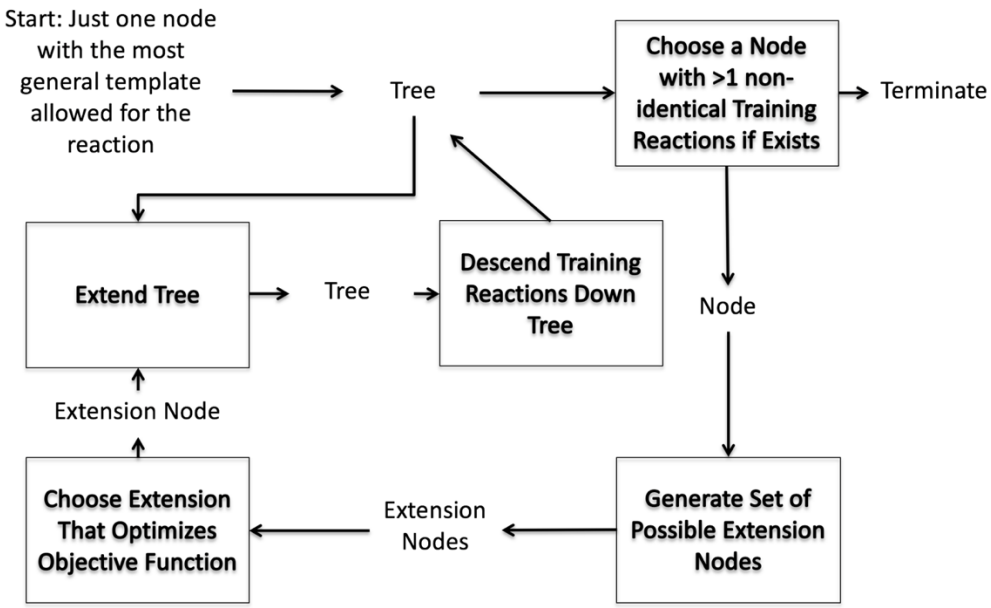

Figure 14. *Decision tree estimator generation algorithm.*

Trees were generated for oxygen substitution, internal endocyclic radical addition, and radical addition. Leave-one-out errors were computed for both original RMG rate rules and each generated tree, as shown in Figure 15. The generated trees are significantly more accurate than RMGs current state of the art rate rules. Prediction accuracy, measured by median absolute error (MAE) factor, root mean squared error (RMSE) factor, and 2-sigma error factor, is consistently improved by a factor of two over original RMG rate rules. For internal endocyclic radical addition, the improvement is closer to a factor of 6-10. For radical addition, the difference isn't quite as stark because rate rule predictions are quite good relative to the data's uncertainty, but MAE was still reduced from 3.07 to 2.01.

Uncertainty estimation was also developed for the decision trees based on fitting a lognormal distribution to the leave-one-out errors at each node. In order to examine performance, the expected error was calculated based on uncertainty estimation and compared with the leave-one-out error to give the histogram in Figure 16. This can't be read like a typical histogram of errors because, in uncertainty estimation, one does not expect the expected uncertainty to be the exact error. However, the fact that it is centered at 0.14 tells us that our uncertainty estimation approach only slightly overestimates errors.

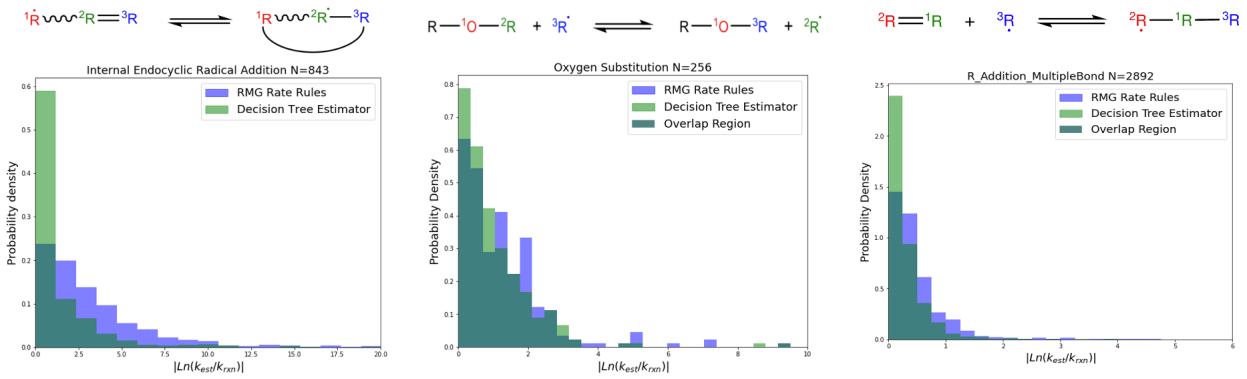

Figure 15. *Histogram of rate estimator errors for internal endocyclic radical addition family (left), oxygen substitution family (middle), and radical addition family (right).*

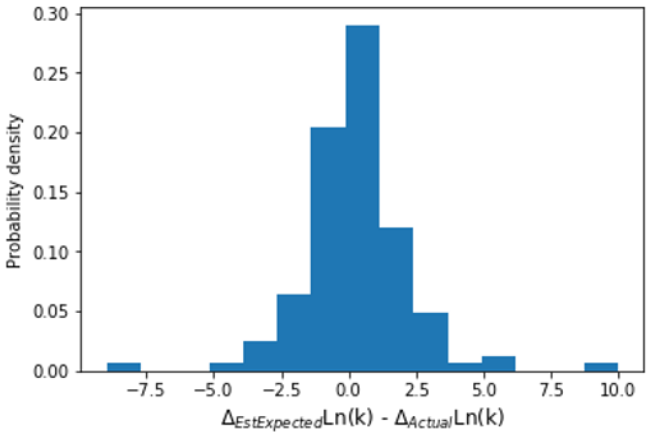

Figure 16. *Histogram of differences for each reaction between expected errors and leave-one-out errors for oxygen substitution.*

Besides implementing the subgraph isomorphic decision tree rate estimator to improve existing rate rules, it was also used as an estimator for the newly created reaction family. As an example, the retro-ene family was added during the work described in Section 4.3.

The addition of this new feature significantly reduced the complexity of designing well-behaving rate rules and allows the estimator's accuracy to improve once new data are available.

4.1.3 Thermochemistry Estimation for Species with Intramolecular H Bonds

We have developed an approach for accounting for hydrogen bonding with group additivity schemes and implemented the change into the RMG code. A hydrogen bond type was added to RMG's molecular structure code, and algorithms were developed to efficiently generate all possible hydrogen-bonded structures from a standard molecule object, as shown in Figure 17. This enables ring strain and energy differences associated with hydrogen bonds to be accounted for by RMG's group additivity and ring strain correction schemes. The Gibbs energy at 298 K of each hydrogen-bonded molecule (and the un-H-bonded molecular structure) can then be calculated using RMG's group additivity thermo estimator and the thermodynamic parameters

associated with the lowest Gibbs energy at 298 K (presumably associated with the lowest energy conformer) can be used.

To generate appropriate groups to improve the accuracy of this scheme, it is necessary to calculate the thermochemical parameters for hydrogen-bonded molecules accurately. This is not easy because intramolecular hydrogen bonds tend to cause tight couplings between rotors within molecules, making standard one-dimensional hindered rotor approaches inappropriate. We developed an algorithm for N-D semiclassical rotor calculations and implemented it in our software Arkane, a package used for calculating thermochemical and kinetic parameters from *ab initio* calculation results. Details will be included in an in-preparation publication on Arkane. An example analysis for the molecule HOCH2CHO that has two rotors are shown in Figure 18. Properly coupling the rotors at high temperatures makes a difference of about 0.6 kcal/mol in this case. Given the expected value of the error in a typical CBS-QB3 calculation is about 1 kcal/mol, and the torsion associated error should scale with the number of rotors, this is a quite significant improvement.

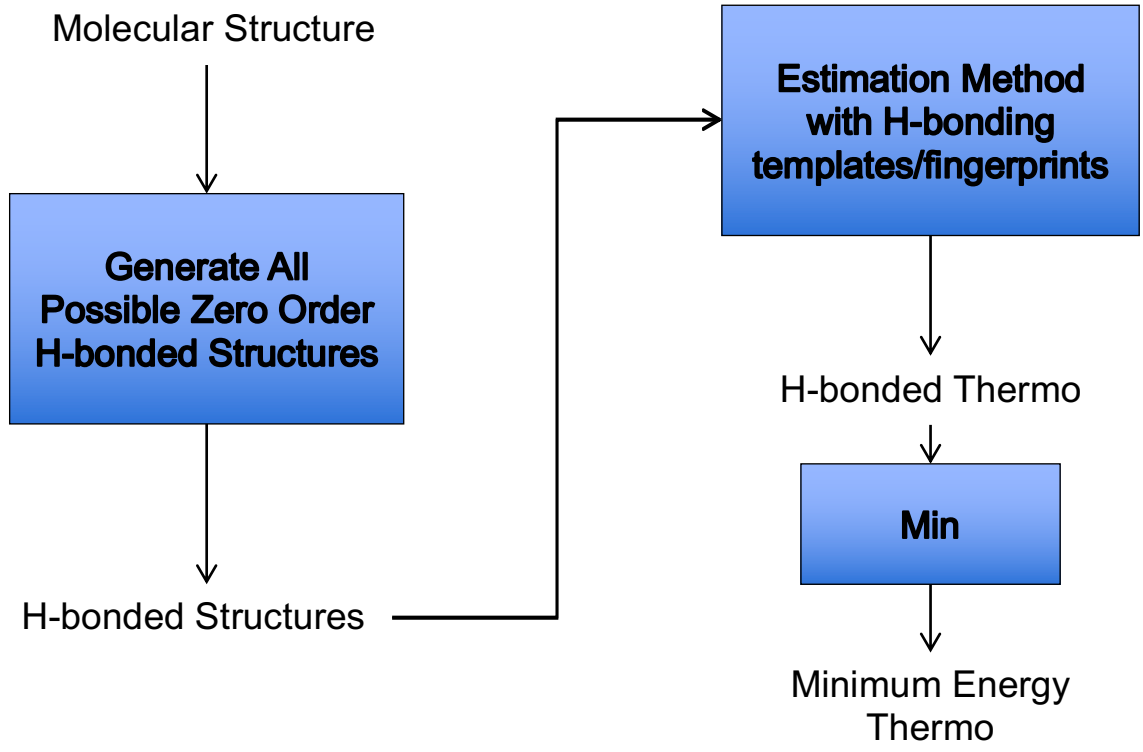

Figure 17. *Hydrogen bonding thermochemistry estimation scheme.*

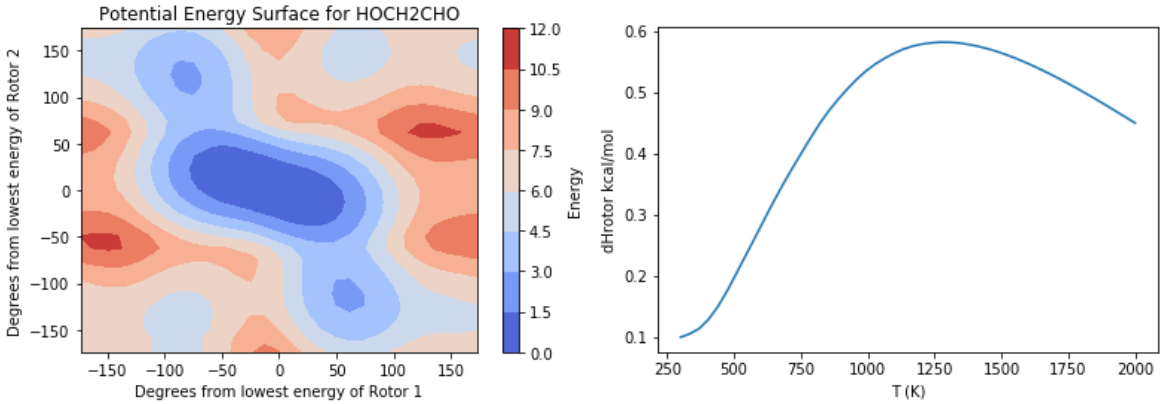

Figure 18. *Left: potential energy surface generated for HOCH2CHO at the MMFF94s level. Right: difference in Enthalpy between treating the two rotors of HOCH2CHO as coupled and independent.*

To demonstrate the effectiveness of the improved workflow, the example of light alkene mechanism generation is shown in Figure 19. As can be seen, the error of the predicted observables is getting smaller with increasing iterations.

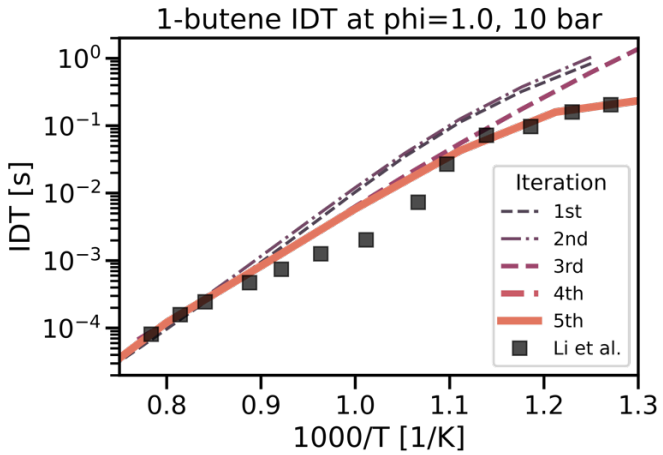

Figure 19. *Experimental and predicted ignition delay time of 1-butene stoichiometric oxidation at different iterations.*

4.2 Models for First Two Biofuels

Models under the scope of the Section 4.2 are models for methyl propyl ether and cyclopentanone.

4.2.1 Methyl Propyl Ether (MPE)

A model was generated for the combustion and pyrolysis of methyl propyl ether (MPE) from 400-1650 K and 0.3-100 bar using the Reaction Mechanism Generator (RMG) package. The model was seeded with the RMG kinetic libraries BurkeH2O2inN2[21] and Klippenstein_Glarborg2016[22] and included accurate thermodynamic data from the following RMG libraries: primaryThermoLibrary, thermo_DFT_CCSDTF12_BAC, CBS_QB3_1dHR, DFT_QCI_thermo,

BurkeH2O2, and Klippenstein_Glarborg2016. As part of the refinement effort, 91 rate coefficients as well as 138 sets of thermochemical parameters were calculated at G4[23] level of theory and included in the model. The model performance was tested on data collected by teams under the Co-Optima project, and the details are included in Section 5.1.1.

Oxidation and pyrolysis kinetic pathways in a plug flow reactor or a shock tube were obtained from simulations at conditions identical to the experiments (details are included in Section 5.1.1), shown in Figure 20, Figure 21, and Figure 22. The flow tube conditions are fairly representative of low-temperature regimes in a rapid compression machine (RCM) or ignition quality tester (IQT), however, under non-IQT conditions, the reactions between radicals and MPE are much less significant.

At low temperatures, MPE loss is dominated by H atom abstraction by OH from hydrogens on the two carbons adjacent to the oxygen. At low enough temperatures, the produced MPE radicals can add oxygen twice before pyrolyzing to generate two OH radicals. At each step, the radicals can also pyrolyze to make one OH or abstract a hydrogen atom from MPE to create a stable species and a new MPE radical. The pathway associated with the central carbon of PME tends to dominate. It is also the most favorable for O2 additions, while the pathway associated with the end carbon bonded to the oxygen tends to pyrolyze more easily. This can make the system highly sensitive to the branching ratio between the two paths in certain temperature regimes, as occurs in some of the flow tube simulations. At higher temperatures, such as in the shock tube, the MPE radicals pyrolyze rather than add oxygen giving a methyl radical + propanal and a propyl radical + formaldehyde, respectively. Additionally, MPE can pyrolyze at high temperatures to produce methanol and propene.

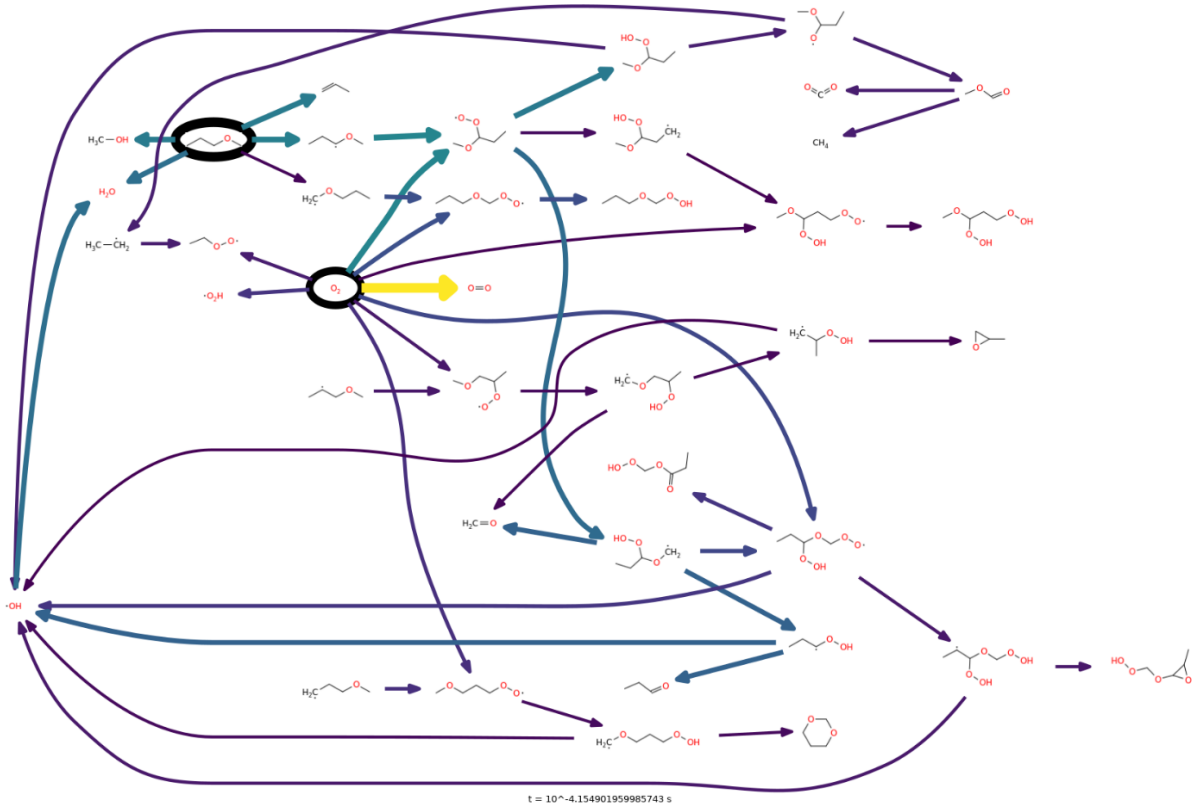

Figure 20. *Flux diagram of an IQT simulation of MPE at 0.0007 sec.*

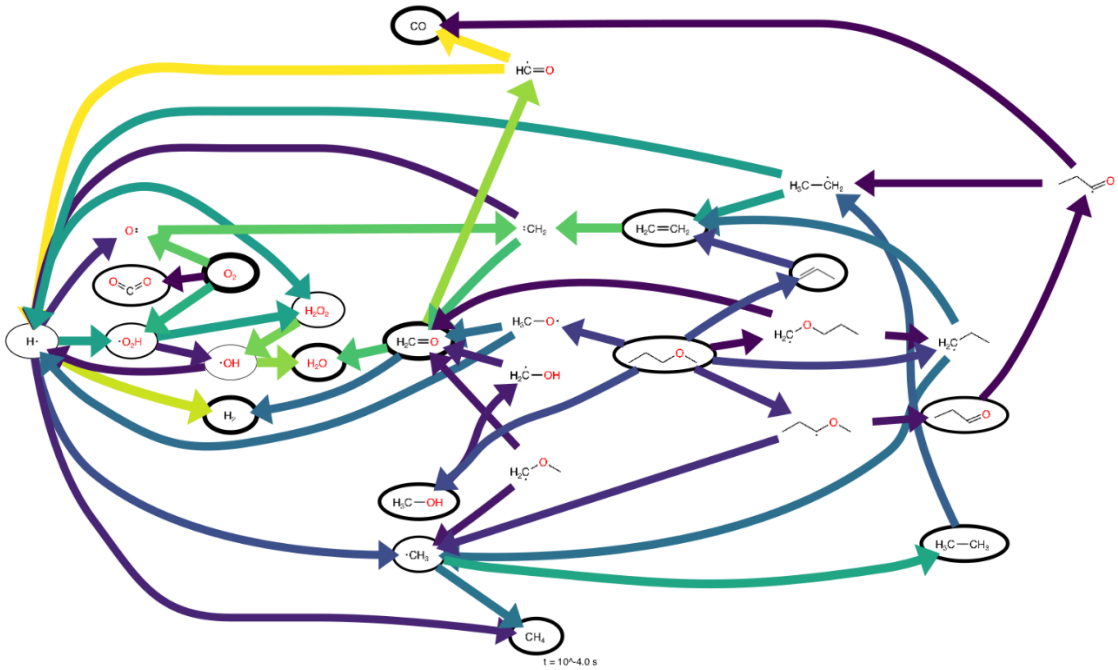

Figure 21. *Flux diagram of MPE shock tube oxidation simulation at 1313 K, 9.01 atm and 0.1 ms.*

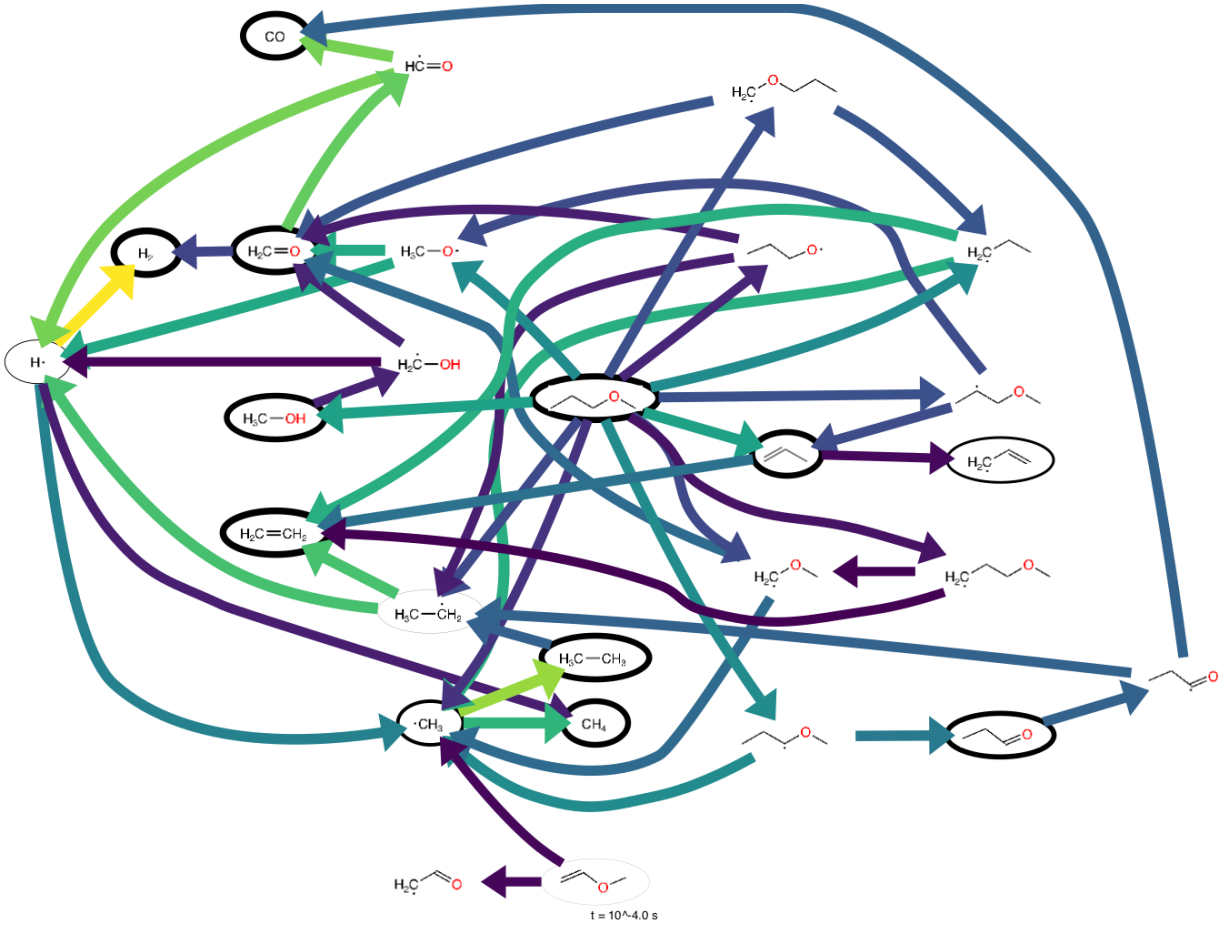

Figure 22. *Flux diagram of MPE shock tube pyrolysis simulation at 1311 K, 9.69 atm and 0.1 ms.*

4.2.2 Cyclopentanone (CPO)

Cyclopentanone modeling was done at MIT mainly focused on two scopes: 1. Quantum chemical calculation for important low-temperature oxidation pathways[3,24], and 2. development of a model for pyrolysis system and understand its key chemistry[25].

For the first scope, *ab initio* calculations at CBS-QB3[26,27] level of theory were conducted on the subsequent pathways from the O_2 addition to 2- and 3-oxo cyclopentyl radicals (Figure 23 and Figure 24) involving reactions from the following families:1. Intramolecular H atom migration; 2. HO2 elimination; 3. Cyclic ether formation from QOOH; 4. Beta scission.

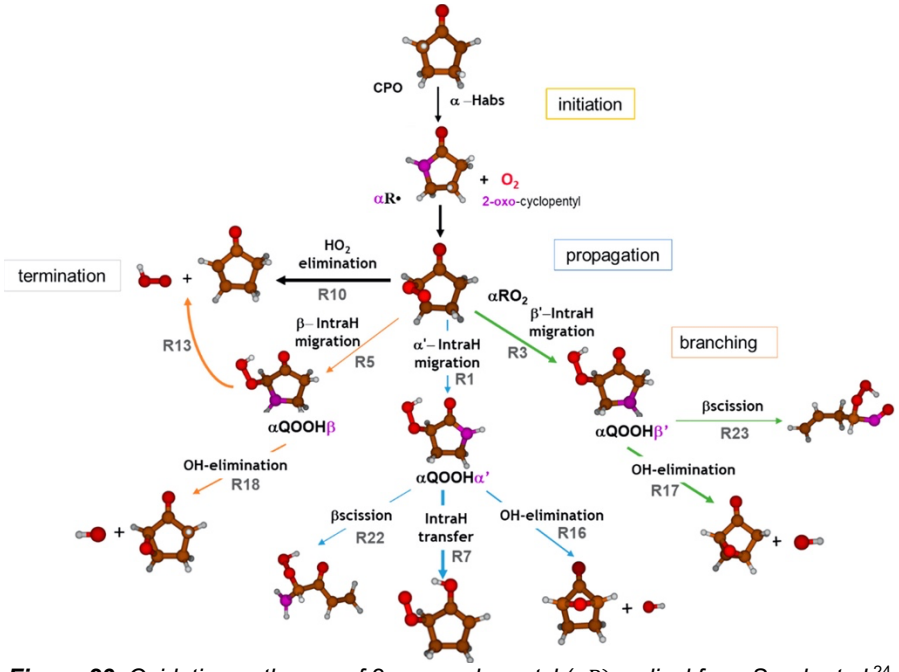

Figure 23. *Oxidation pathways of 2-oxo-cyclopentyl (αR) radical from Sarah et al.*[24]

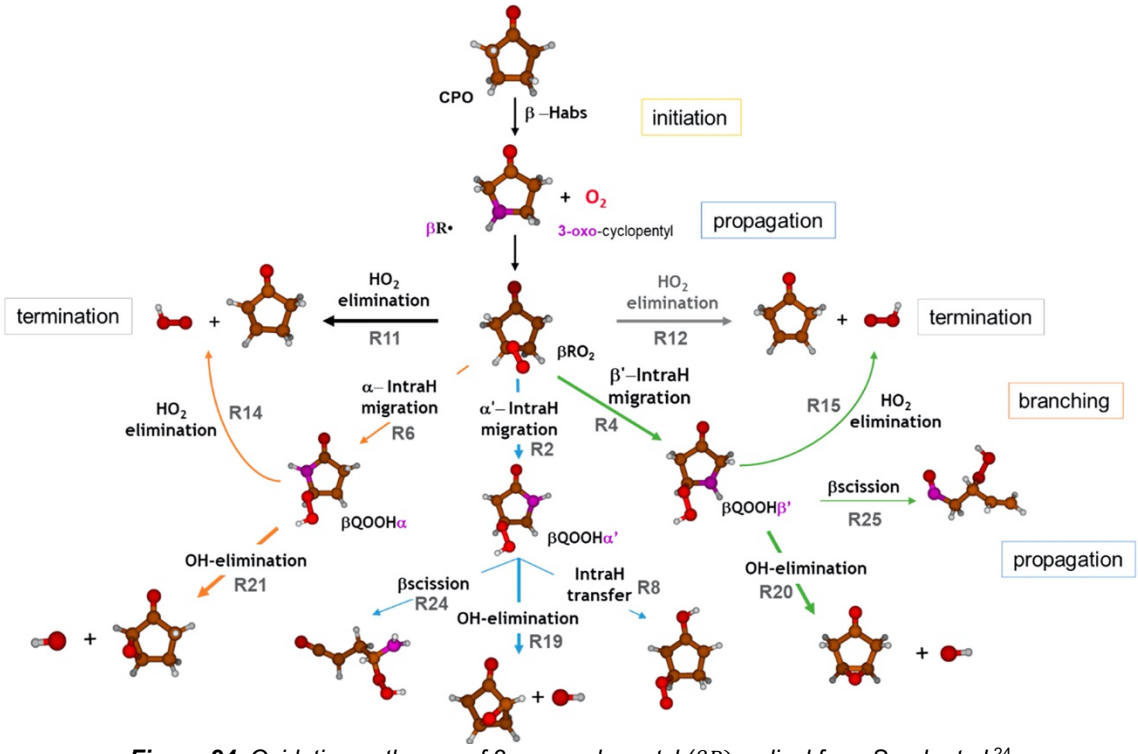

Figure 24. *Oxidation pathways of 3-oxo-cyclopentyl (βR) radical from Sarah et al.*[24]

The exploration conducted by this study on those pathways were both novel and comprehensive. For the first time, it provided the thermodynamic data and rate coefficients for those low-temperature isomerization and branching pathways. From obtained data, the study showed that the inclusion of the carbonyl group increases the reaction barrier for isomerization reactions due

to the rigidity of the sp2 hybridization carbon. In contrast, it results in lower barriers for HO_2 elimination reactions due to the conjugate effect compared to the cyclopentane counterpart. The study also exhibited differences in the kinetic behavior of α and β −substituted cyclopentanone. The obtained results from this study not only provided accurate data for important CPO chemistry, which filled the gap in kinetic modeling, but they also contributed to a better understanding of kinetics for cyclic fuel species.

For the second scope, we developed a comprehensive kinetic model for high-temperature pyrolysis of cyclopentanone and validated this mode by high-pressure shock tube (HPST) experiments. And this result was selected as one of the Co-Optima FY20 Highlights.

To build the model, we first refined the rate of the most sensitive reaction (CPO -> CO + 2 C_2H_4) with the highest affordable level of theory (CCSD(T)-F12/cc-pV{T,Q}Z-f12//APFD/6-311+G(2dp)) (shown in Figure 25). With this rate, secondary reaction rates published by Zhou et al.[28], and in-house calculation for other missing decomposition reactions, we developed a detailed kinetic model for pyrolysis system using the Reaction Mechanism Generator (RMG)[29] package. The model's prediction had a good agreement with the experimental data for mole fractions and branching ratio (Figure 26), while the experimental details can be found in Section 2.1 and 5.1.2.

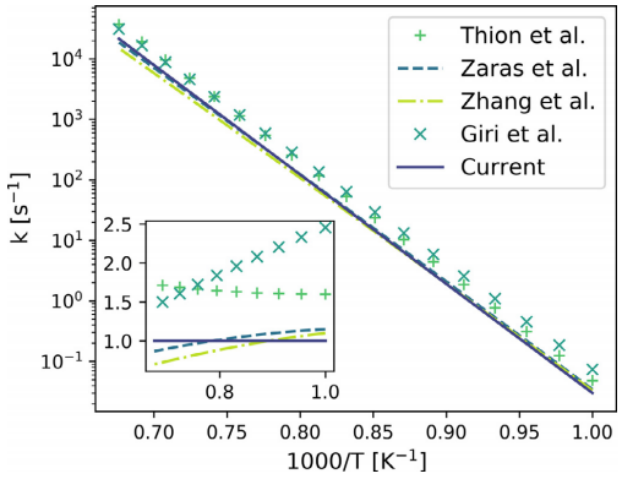

Figure 25. *High-pressure-limit rate coefficients of reaction (CPO -> CO + 2 C_2H_4) from different sources[3,6,30,31] from Xiaorui et al.[25]. The inset shows the rate coefficient values at different temperatures relative to the rate coefficient calculated in the current work.*

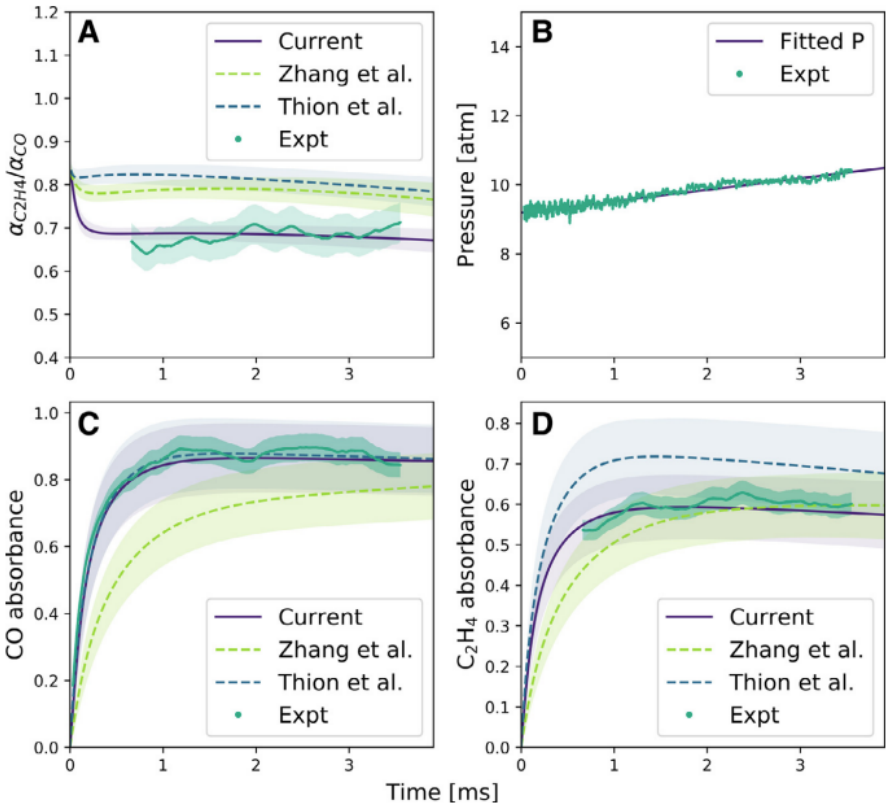

Figure 26. *HPST experiments results at T_5 = 1393K, P_5 = 8.98 atm and $x_{CPO,0}$ = 4000 ppm. (A) $\alpha_{C2H4}/\alpha_{CO}$; (B) pressure; (C) CO absorbances; (D) C_2H_4 absorbances. For (A), (C) and (D), the purple solid lines are the predictions from the current model, while the blue and green dashed lines are predictions from Thion et al.*[6] *and Zhang et al.*[3] *models., respectively, and the green dotted lines are experimental data. The uncertainty of each curve is indicated by the translucent region with the same color as the curve. For (B), the green dotted line is the measured pressure, while the purple line is the pressure fitted to the measurement used as the boundary condition for the ideal-gas adiabatic simulation.*

The obtained model suggested that radical-involved pathways play essential roles in the CPO decomposition, as shown in Figure 27. During the early stage, when H radicals are accumulating, the radical-involved decomposition pathways are activated and become as crucial as the unimolecular pathway. During the transition stage, reactions involving radicals and products become as important as reactions involving radicals and CPO due to the product accumulation, resulting in a decreasing x_{H}. During the product pyrolysis stage, the decomposition of the mixture of C_2H_4 and other products becomes dominant as CPO is depleted. Findings in this study contributed to the understanding of pyrolysis of CPO and established a more comprehensive combustion/pyrolysis model. Such understanding can also be helpful when proposing pyrolysis or combustion models for other biofuels.

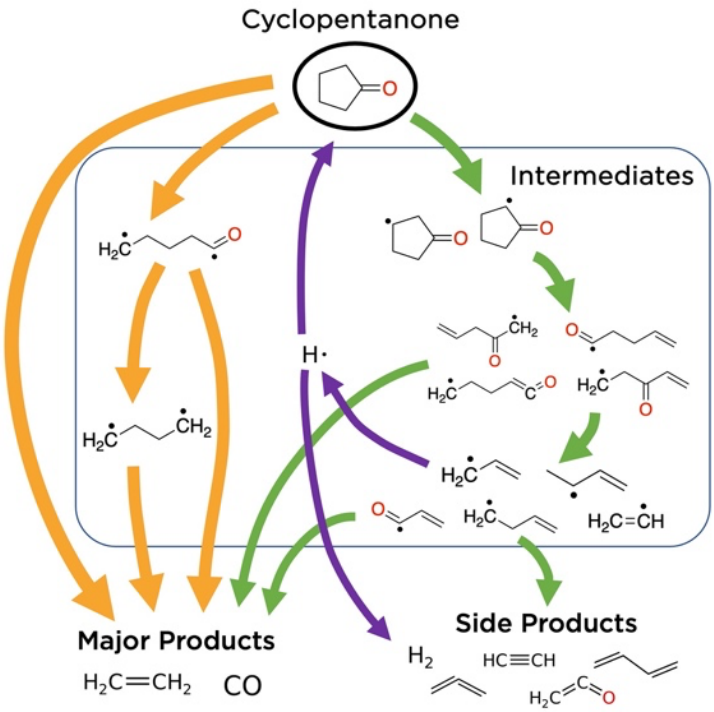

Figure 27. *Dominant reaction pathways of cyclopentanone pyrolysis at high temperature. The unimolecular pathways are colored orange, and radical-involved bimolecular pathways are indicated by green and purple.*

4.3 Models for Next Four Biofuels

The models developed under Section 4.3 are the models for butyl acetate isomers, namely normal-, iso-, secondary, and tertiary-butyl acetates (or in short, nBA, iBA, sBA, and tBA). A manuscript about combustion chemistry for these isomers is now being prepared.

The model construction process was generally based on the workflow proposed in the scope of Section 4.1. In each iteration, four different models were generated by RMG package[29] on the basis of RMG libraries and parameters from in-house quantum chemistry calculations; generated models were then analyzed by sensitivity and rate of production (ROP) analysis to figure out potential parameters (thermochemical data and rates) that could significantly contribute to model uncertainties; identified species will be fed to the automatic rate calculator (ARC) package[32] for thermodynamic property calculation, and reactions will be calculated manually with the assist of QM packages; All calculations were at CBS-QB3 level of theory; the updated parameters were collected and used as input for further model generation.

On top of the normal workflow, we first developed a high-quality light alkene sub-mechanism, as light alkenes and their oxidated derivates were important intermediates in the BA oxidation systems. A comprehensive literature review was first done on rates of critical reactions to ensure as many high-quality parameters were used. RMG was then used to develop the light alkene sub-model. The overall estimation quality of the generated mechanisms was then assessed by the fractional bias (FB) and normalized mean square error (NMSE), along with other published models, shown in Figure 28. Based on the evaluation, it is possible to conclude that the sub-mechanism was the most accurate model among the ones analyzed for alkenes combustion. The

purely theoretical basis for model development, together with the absence of corrective factors, makes the produced mechanism a desirable building block for the more complicated butyl acetate model.

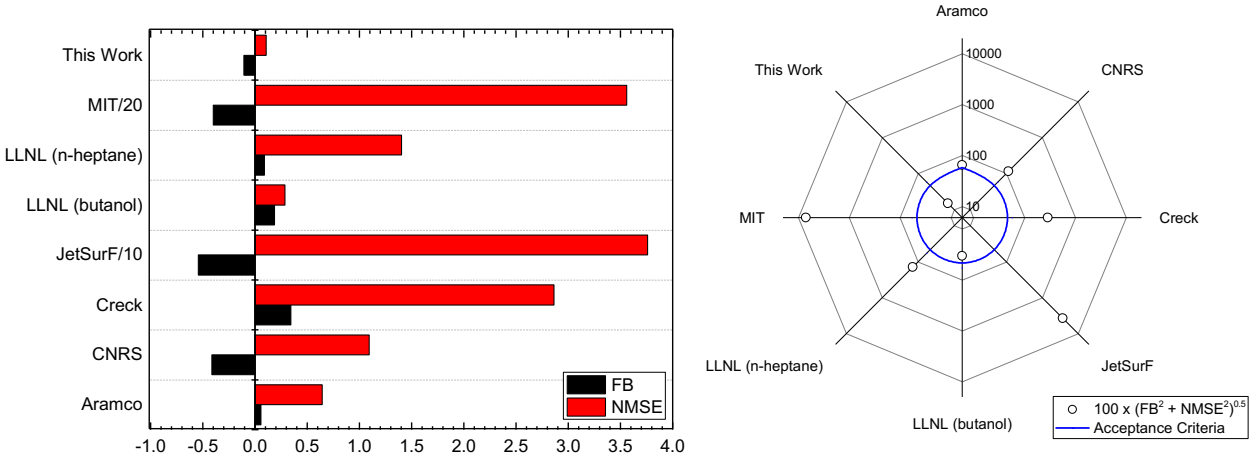

Figure 28. *Evaluation of the overall estimation quality for models covering light alkene*[33–39]*, in terms of fractional bias (FB) and normalized mean square error (NMSE). For the sake of proper visualization, NMSE values for JetSurF and MIT were reduced by a factor of 10 and 20, respectively.*

Besides developing a sub-mechanism, we created new rate rules for the retro-ene reaction family by the approach of subgraph isomorphic decision tree, as described in Section 4.1.2. The training data for the retro-ene rate rules are mostly rates calculated in-house at CBS-QB3 level of theory. Although the primary motivation is to provide accurate rates for BA retro-ene reactions, the rate rules' training set eventually covers a wide range of reactants: esters, ethers, peroxides, and species with carbonyl groups. A partial list of the training reactions is shown in Figure 29. The introduction of retro-ene rate rules to RMG allows retro-ene reactions to be generated during the reaction network enlargement process. The training reactions' diversity ensures reasonable rate estimations for predicted retro-ene reactions that had never been investigated before.

Other than parameter calculations used to train rate rules, calculations were also conducted on the primary reactions, namely H atom abstraction of butyl acetate isomers by OH and HO2 radicals.

According to our model, all butyl acetate isomers have two major categories of primary reactions: H atom abstraction reactions and retro-ene reactions. The branching ratio is determined by both temperature and the alkoxyl group structure: retro-ene reactions are more prone to take place at higher temperature due to their higher activation barriers; they are more prone for more substituted alkoxyl group due to weaker C-O bonds. Differences in the branching ratio further impact the dominant pathways and combustion properties (e.g., ignition delay time), as shown in Figure 30.

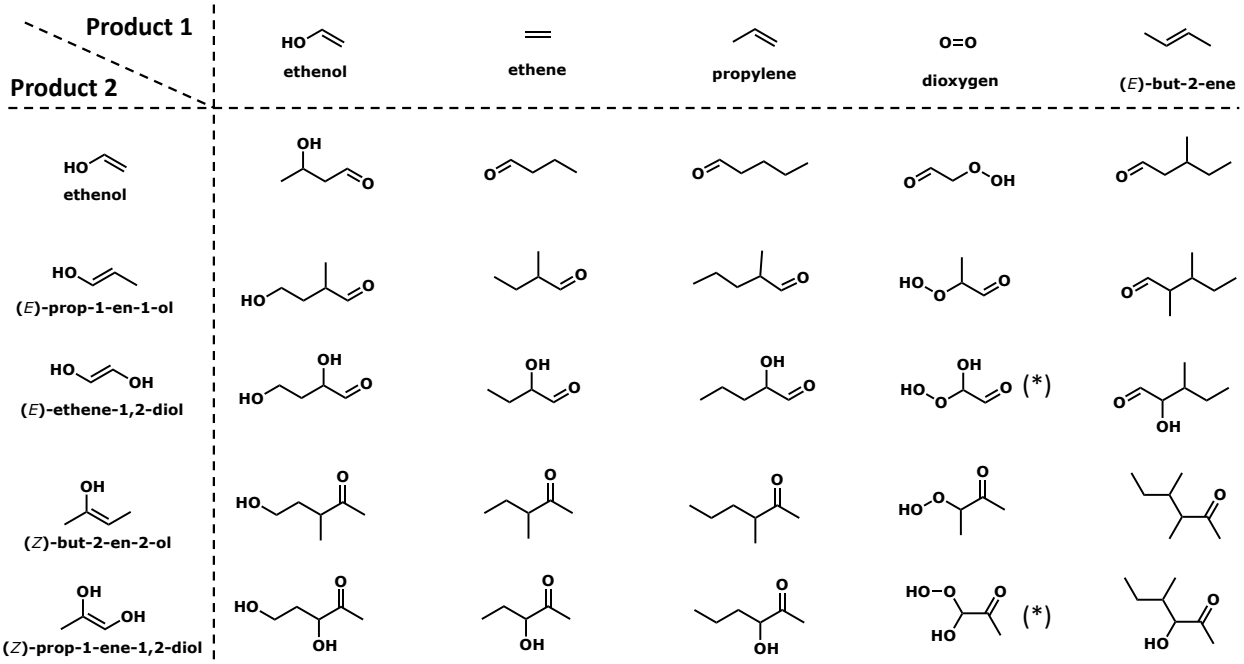

Figure 29. *A partial list of retro-ene reactions with rate coefficients calculated under the scope of this project. The reactants are listed in the main sheet while the products can be found in the first row and first column. Searching for transition states and rate coefficient refinement was unsuccessful for reactants marked with (*).*

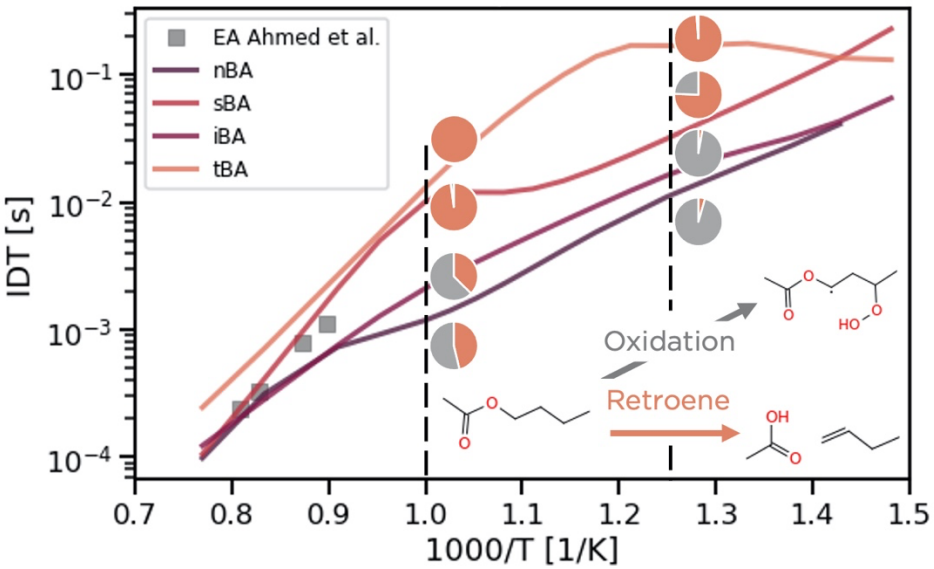

Figure 30. *The temperature dependence of ignition delay time and branching ratio of butyl acetate (BA) isomer oxidation at phi = 1.0, P = 10 bar. The branching ratios shown as pie plots are values at half of the time when BA is depleted. Ethyl acetate (EA) is used as a reference for comparison.*

A flux diagram that provides a graphical illustration of the major reactions and pathways is shown in Figure 31. Generally, a model for BA isomers consists of

- Primary H atom abstraction and retro-ene reactions
- Sub-mechanisms of acetic acid and butene isomers to account for high-temperature oxidation and pyrolysis
- Generation, isomerization, and decomposition reactions of butyl acetate peroxides
- A sub-mechanism of butanal isomers to account for low-temperature oxidation

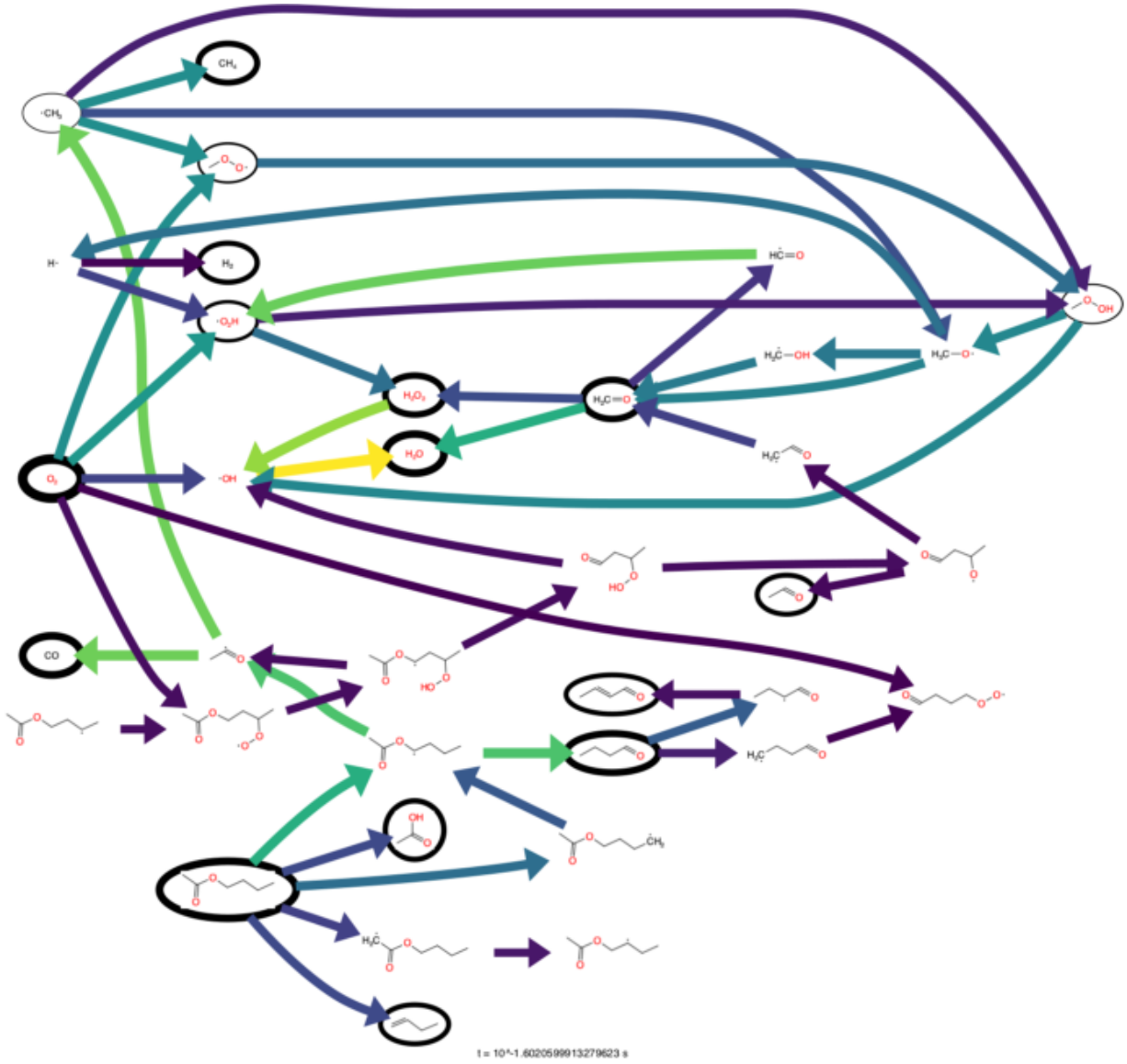

Figure 31. *Flux diagram of nBA oxidation at the condition of 800 K, 10 atm, phi = 1.0. It includes major fluxes right before the ignition delay.*

4.4 Models for Remaining Biofuels

The remaining models are the models for 3,3- and 3,4-dimethylpent-1-ene, 1-octene, and 2,3-dimethylbut-2-ene.

4.4.1 3,3- and 3,4-dimethylpent-1-ene

We constructed combustion models for both 3,4-dimethylpent-1-ene (tfDMP) and 3,3-dimethylpent-1-ene (ttDMP) using the Reaction Mechanism Generator (RMG). Models were constructed covering a temperature range of 650 – 1200 K, and a pressure range of 3.0 - 110.0 atm; a stoichiometric air-fuel ratio was considered as the initial condition and 99% conversion of the fuel was set as the termination condition for each simulation during the model generation. In order to improve the accuracy of the model, thermodynamic parameters were refined based on quantum mechanical (QM) calculations at CBS-QB3 level of theory. In total, 336 and 215 species were calculated for ttDMP and tfDMP, respectively. Moreover, rates for retro-ene primary reactions were also calculated. The final model for ttDMP consists of 902 species and 19,996 reactions, while the tfDMP combustion model consists of 904 species and 17,639 reactions. Before publishing these models, more investigations have been done to understand the chemistry, especially the link between the phi sensitivity and microscopic kinetic and molecular geometry information.

Both fuels were reported as phi-sensitive fuels, meaning minor differences in the fuel-air ratio could cause significant changes in combustion process observables. The time-histories of OH radical mole fraction at 0.5,1.0 and 1.5 fuel-air ratios and various temperatures are shown in Figure 32. The developed models were able to capture this phenomenon: the peak time of the OH mole fraction at leaner conditions was different from the time at stoichiometric and rich conditions by more than an order of magnitude. Moreover, the model also captured the multi-stage ignition behavior at leaner conditions. Besides, by summarizing ignition delay times in a single graph, a negative temperature coefficient (NTC) region within the 650 – 900K could be observed (Figure 33). An example flux diagram that includes low-T oxidation branching pathways of ttDMP is shown in Figure 34.

4.4.2 1-octene

A 1-octene model was initiated in the year 2020 to study its phi sensitivity phenomenon and developed for two iterations according to the improved workflow as described in Section 4.1 before the pandemic of COVID-19. However, due to resource constraints and limitations in cooperation, we had to postpone developing the 1-octene mechanism that was relatively better-studied compared to other molecules. The model was not finalized at the closure of this funding.

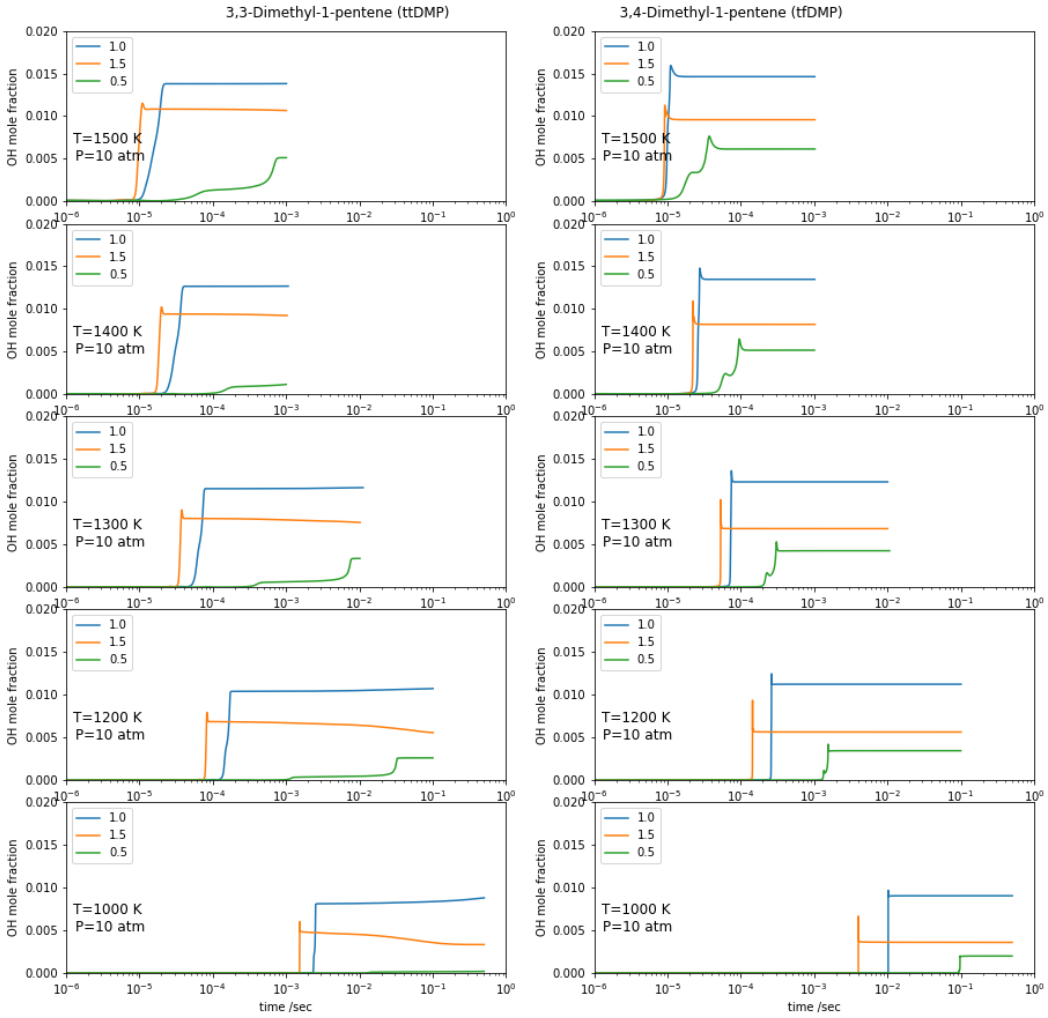

Figure 32. *Time-histories of OH radical mole fractions at 1000 – 1500 K and 0.5, 1.0, 1.5 fuel-air equivalence ratios.*

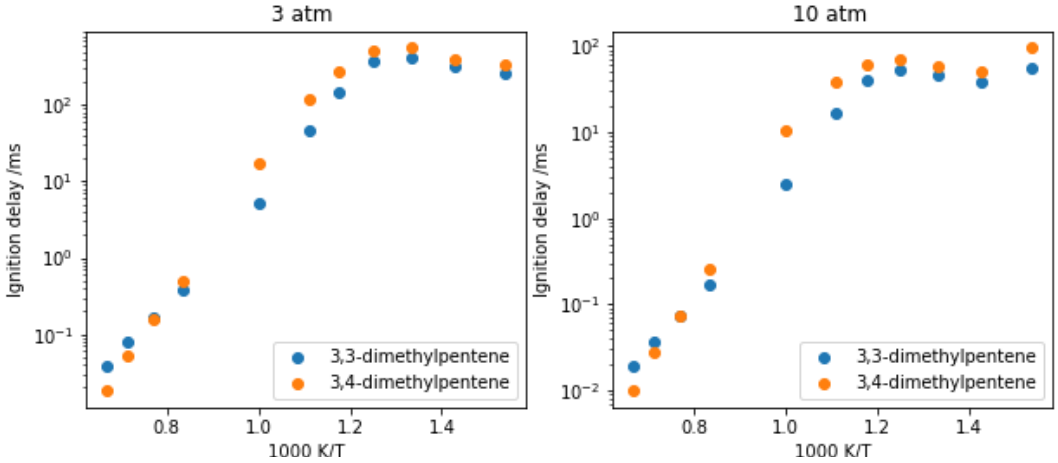

Figure 33. *Ignition delay times for ttDMP and tfDMP at 3 and 10 atm with equivalence ratios of 1.0.*

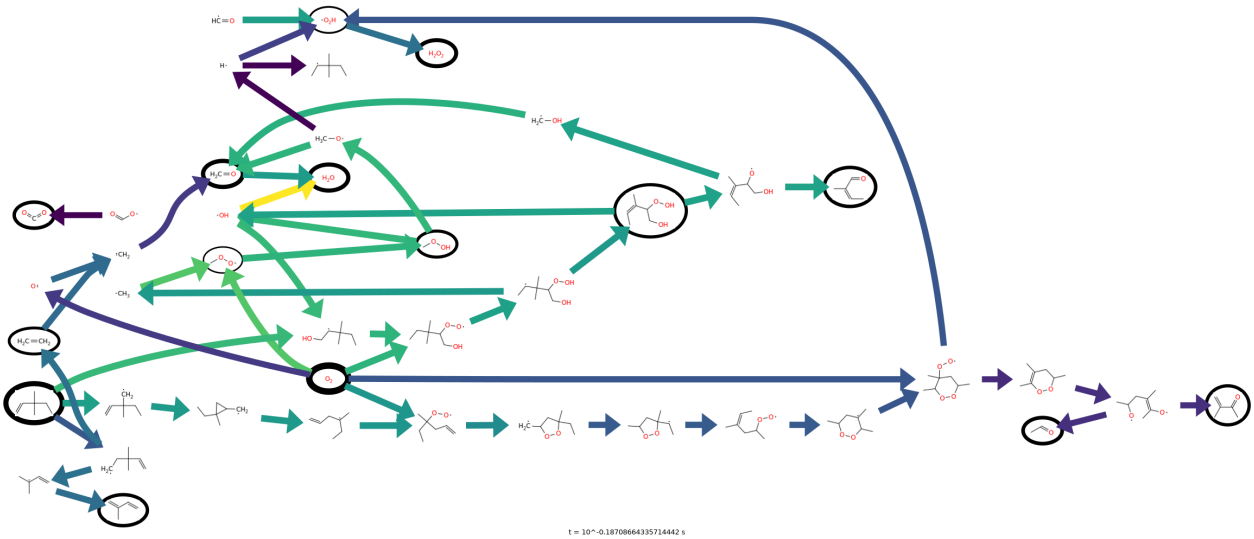

Figure 34. *Flux diagram of 3,3-dimethylpentene at (T = 650 K Pressure=10.0 atm) before the ignition (0.65 s).*

4.4.3 2,3-dimethylbut-2-ene (23DMB)

2,3-dimethylbut-2-ene (23DMB) is a biofuel that shows the hyper-boosting effect: a mixture consisting of 23DMB and another blendstock may yield a higher research octane number (RON)[40] than the RON of either component. A 23DMB combustion model was developed and a great amount of effort was put into the refinement of the parameters. While the model construction is not finalized, a manuscript about this model and involved calculations is being prepared while writing this report.

The model was generated by the same workflow mentioned in Section 4.1 by RMG with the same simulation conditions used in the other model generation process. At current stage, the generated model has 926 species and 40964 reactions, with over 400 sets of accurate thermochemical data calculated and tens of key reaction rates from quantum chemistry results at CBS-QB3 level of theory. Besides rates specific to 23DMB modeling, effort was also put into updating the rate rules for cyclic ether formation reactions and O[O] intramolecular addition reactions.

A reaction pathway diagram is shown in Figure 35, which clearly shows the R -> ROO -> ROOH -> OOQOOH pathways that are the major chain branching pathways in most hydrocarbon combustion systems. Besides, a pathway initiating from HO2 addition to 23DMB and yielding OH radical and an oxygenated intermediate can be found, converting less reactive HO2 species to more reactive OH species. It can be a potential cause of the hyper-boosting effect and needs further investigation.

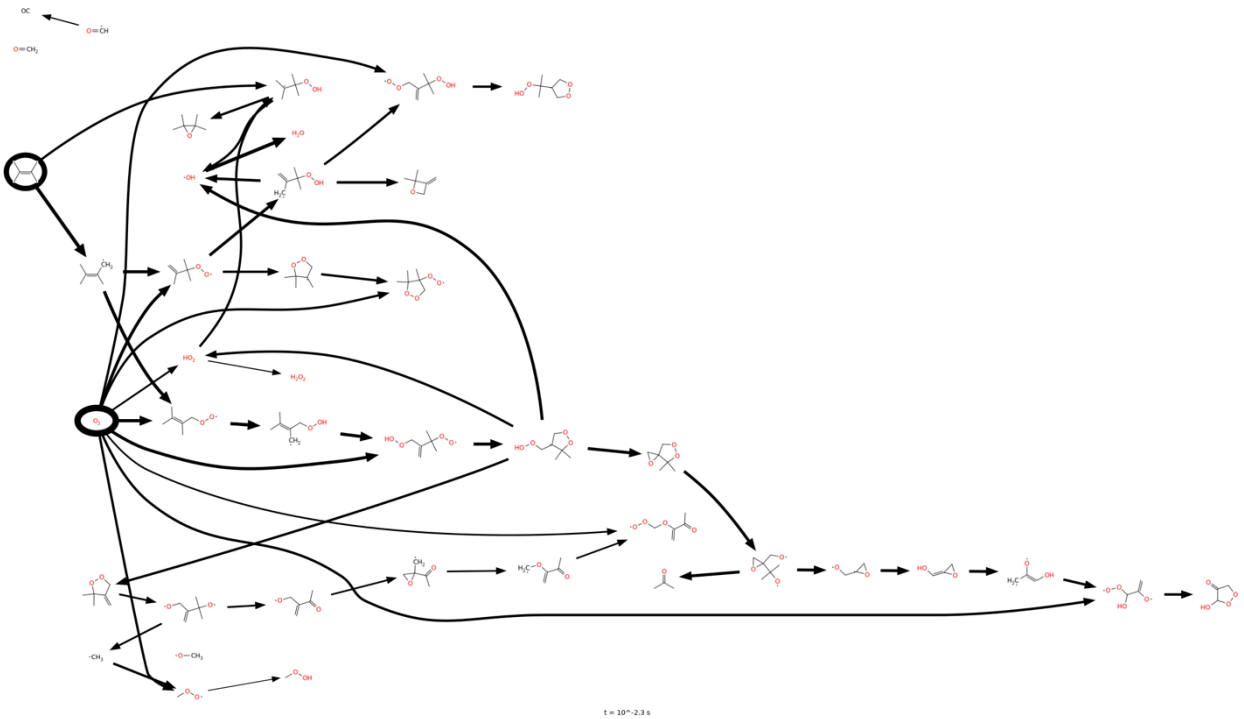

Figure 35. *Flux diagram of 23DMB at (Temperature= 700 K Pressure=10.0 atm, phi = 1.0) slightly earlier than ignition delay time (4 ms).*

Moreover, along with the effort of 23DMB modeling, quantum chemistry calculations were done on prenol reactions, the only Tier 3 biofuel exhibiting hyper-boosting effect. This was part of the collaboration with other teams under the Co-Optima project on the prenol modeling, and it was believed to be helpful for 23DMB modeling.

Chapter 5 Model vs. Experimental Validations

In Chapter 4, we described how we used the computer to rapidly construct accurate kinetic models for several proposed biofuels. In this section, we report experimental measurements we made to validate and test the accuracy of the computer models. Many of the experimental data were measured in experiments performed at the University of Central Florida that used a shock wave to jump the temperature up to combustion-relevant conditions, and monitored the time-dependent formation and consumption of predicted reaction intermediates using methods described in Chapter 2 and Chapter 3.

5.1 Validate Y1 Models vs Experiments

Validation for Y1 models includes: 1. the validation of the methyl propyl ether model, and 2. the validation of cyclopentanone models.

5.1.1 Validation of the MPE Model

Model performance was tested on shock tube data collected at the University of Central Florida (UCF), flow tube data collected at the National Renewable Energy Laboratory (NREL), and rapid compression machine data collected at Argonne National Laboratory.

For the shock tube data, the model agrees quite well with the experiment. At oxidative conditions, peak times agree within about 50%, and peak heights agree within about 34% of the experiment (Figure 36). The performance on pyrolysis conditions is equally agreeable well within the uncertainties of the experiment and the model (Figure 37).

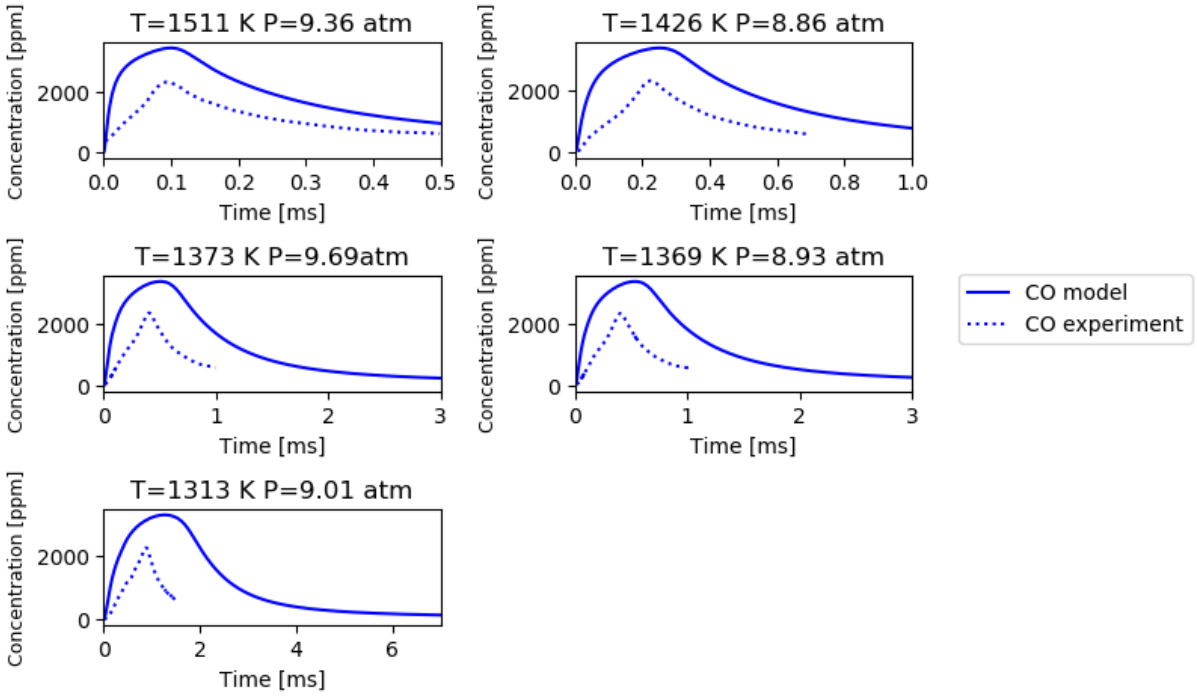

Figure 36. *Comparisons between the model prediction and shock tube experimental data for the system of MPE oxidation at various conditions.*

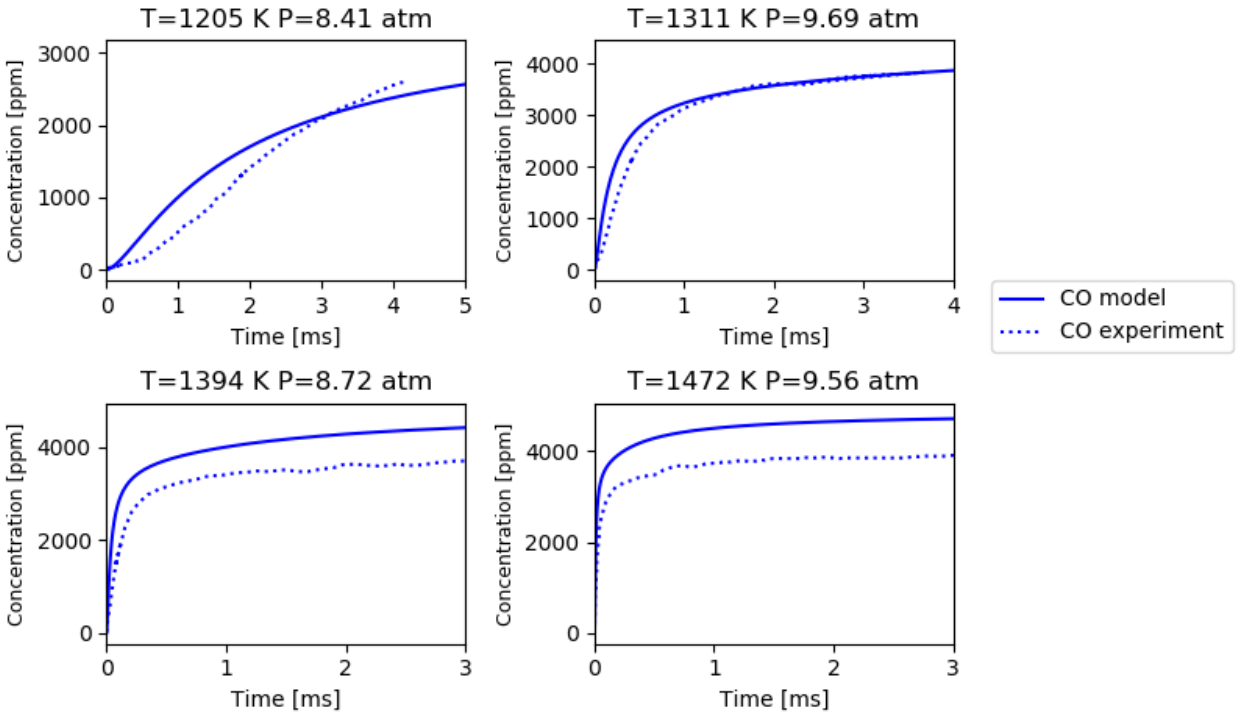

Figure 37. *Comparisons between the model prediction and shock tube experimental data for the system of MPE pyrolysis at various conditions.*

The flow tube simulations predict a 25-50 K earlier transition from the low to high PME conversion regime than the experiments, as shown in Figure 38. This is very likely due to the uncertainty in the branching for MPE between the reactions below

$$\mathrm{MPE} + \mathrm{OH} \rightarrow \mathrm{CO[CH]CC} + \mathrm{H_2O}$$
$$\mathrm{MPE} + \mathrm{OH} \rightarrow \mathrm{[CH2]OCCC} + \mathrm{H_2O}$$

At the temperatures of interest, the first reaction has a more active OH feedback loop and leads to more OH production than the second reaction. The sensitivity of PME mass fraction to the rate coefficient for the first reaction has an enormous sensitivity of -5.5. Comparing the 2 sec and 5 sec data, the MPE decay rate is off by about a factor of 2. Extrapolating the sensitivity linearly, this implies that achieving better than the current accuracy predictions would require the rate coefficient for the first reaction to be known within 20%. This might be done with a cleverly designed experiment but would not be an easy task and was beyond the scope of this project. This made it impractical to improve MPE conversion predictions beyond those presented here.

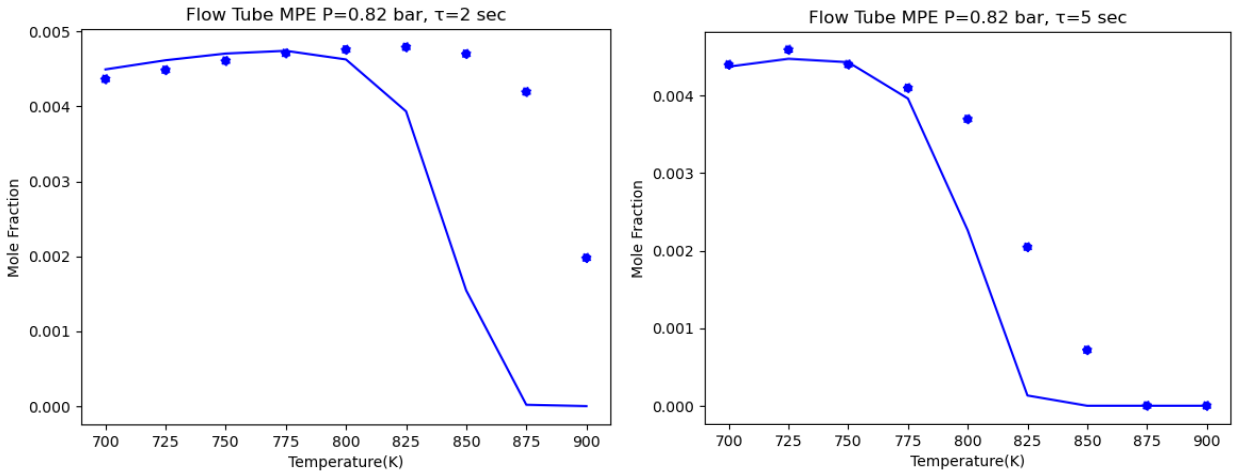

Figure 38. *Predicted and measured mole fractions of MPE exiting the flow reactor at 2 s residence time (left, high flow rate) and 5 s residence time (right, low flow rate).*

The mole fractions of flow tube products are shown in Figure 39. Where the conversion predictions agree, methane, propene, ethene, and propanal agree with the experiments at most points. Acrolein and CO2 are significantly underpredicted at 2 seconds but are much closer at 5 seconds. Ethane is underpredicted in both cases. CO is slightly overpredicted at both conditions.

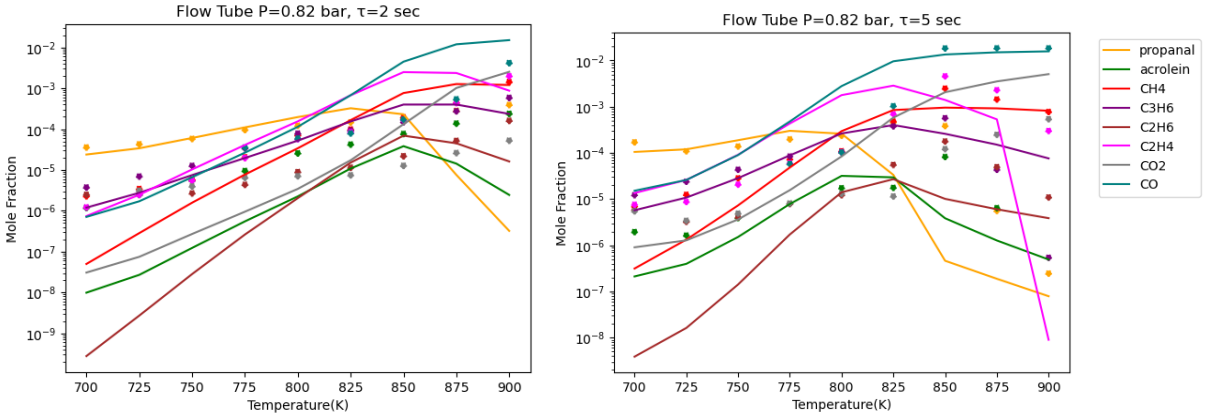

Figure 39. *Predicted and measured mole fractions of major products exiting the flow reactor at 2 s residence time (left, high flow rate) and 5 s residence time (right, low flow rate).*

Rapid compression machine predictions required the simulation using experimental volume traces to achieve accuracy due to the high reactivity of MPE at low temperatures, as shown in Figure 40. Agreement between model and experiment is quite good and never larger than a factor of two (except for two points in the 10 bar experiments) well within the uncertainties of the measurements and model parameters. The unusually large sensitivity of ignition delay to pressure is associated with two chemistry differences. In the dominant O2 feedback loop, the bimolecular second O2 addition to MPE competes very closely with the pyrolysis of the associated radical. At higher pressures, the bimolecular path is about two times faster, leading to a very significant increase in the production of OH radicals, which further results in faster ignitions. Additionally, at higher temperatures, when propanal is being consumed, the product species CCO[O] tends to react bimolecularly:

$$CCO[O] + HO_2 \rightarrow CCOO + O_2$$

Rather than unimolecularly:

$$CCO[O] \rightarrow C_2H_6 + HO_2$$

The first pathway broadly converts two HO2 radicals into two much more reactive OH radicals (accelerating ignition), while the latter simply regenerates the HO2 radical consumed from reacting with propanal.

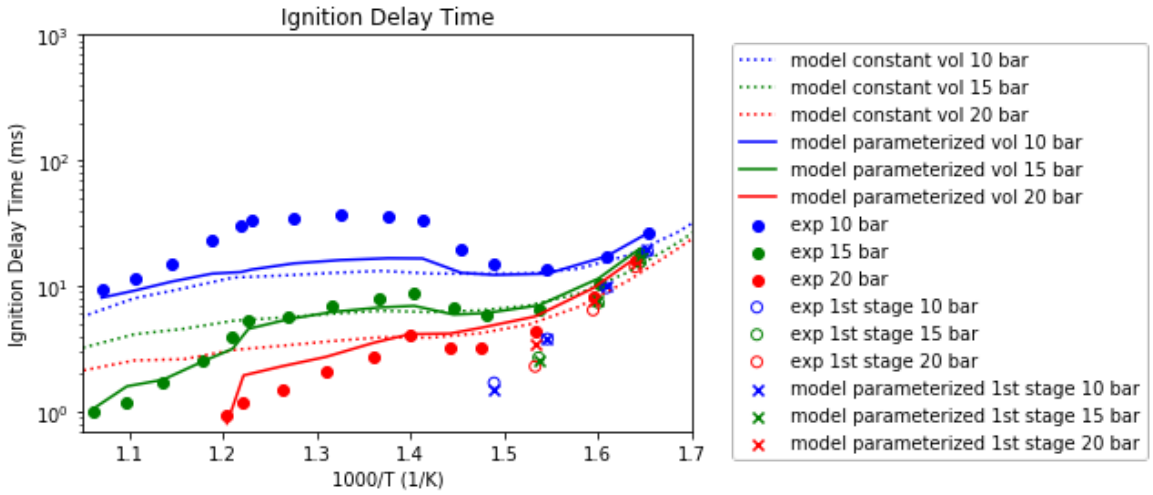

Figure 40. *Measured and model-predicted ignition delay time and end-of-first stage times. Parameterized models account for heat losses and changes in the adiabatic core volume using the measured pressure time history for non-reactive mixtures.*

5.1.2 Validation of the CPO Pyrolysis Model

In order to validate the pyrolysis model, high-pressure shock tube (HPST) measurements were conducted. The time-histories of carbon monoxide (CO), ethylene (C_2H_4), and cyclopentanone (CPO) absorbances over the temperature range of 1156 - 1416 K and pressure range of 8.53 - 10.06 atm were measured. Details on the experimental setup can be found in Chapter 2 and 6 of this report, previous quarterly reports, and in the publications supported by this project.

Species absorbances instead of measured mole fractions were used as the validating metrics. By this approach, the influence of initial condition uncertainties on species distribution can be clearly illustrated, making the validation more robust. Moreover, the correlations among temperature, pressure, and mole fractions are obtained from simulations to correctly calculate the uncertainty propagation, yielding a more accurate uncertainty analysis. Our model was in good agreement with the experimental results between 1217 and 1416 K, as shown in Figure 41.

More insights about the mechanisms can be unveiled by considering the time-histories of C_2H_4 absorbance, especially the absorbance ratio between C_2H_4 and CO ($\alpha_{C_2H_4}/\alpha_{CO}$). $\alpha_{C_2H_4}/\alpha_{CO}$ can be regarded as a substitute for the mole fraction ratio between C_2H_4 and CO ($x_{C_2H_4}/x_{CO}$), which is related to the branching ratio of the system. Further, from the validation point of view, we find that $\alpha_{C_2H_4}/\alpha_{CO}$ is much less sensitive to the uncertainties of initial conditions than species absorbances. We did brute force uncertainty analyses on initial conditions using the current model.

Time-histories of $\alpha_{C_2H_4}/\alpha_{CO}$ as well as the CPO, C_2H_4, and CO absorbances are shown in Figure 42, demonstrating our model is in good agreement with the experimental results. In contrast, the Thion et al. and Zhang et al. models show an overestimation of the $\alpha_{C_2H_4}/\alpha_{CO}$. With this data, we were able to confirm the hypothesis that radical-involved pathways play a major role in the pyrolysis of cyclopentanone, highlighted through the ratio of C_2H_4/CO provided,

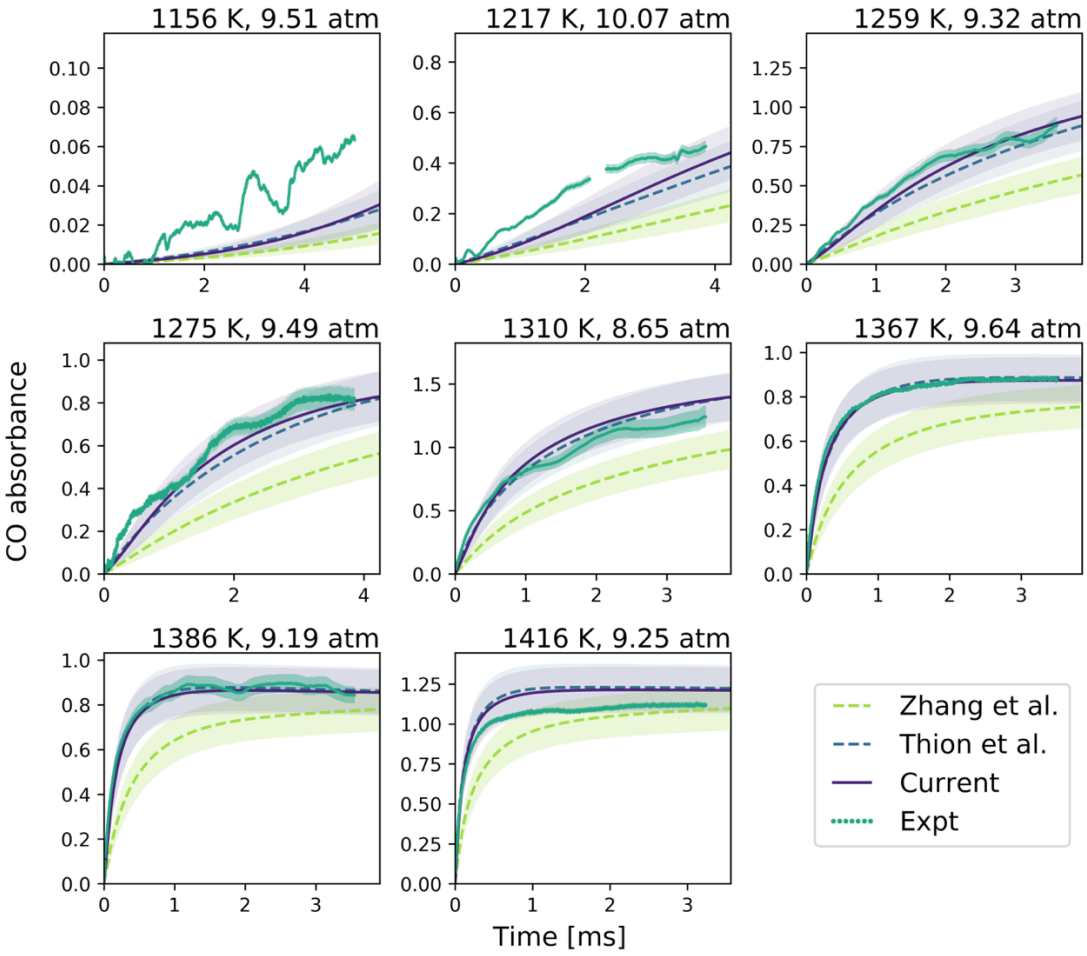

Figure 41. *Time-histories of CO absorbance at different temperatures and pressures. The green dotted lines are experimental results, the purple lines are predictions from the current model, while the blue and green dashed lines are predictions from the Thion et al.*[41] *and Zhang et al. models.*[3] *The temperature and pressure are indicated at the top-right corner of each figure. The uncertainty of each curve is indicated by the translucent region with the same color as the curve.*

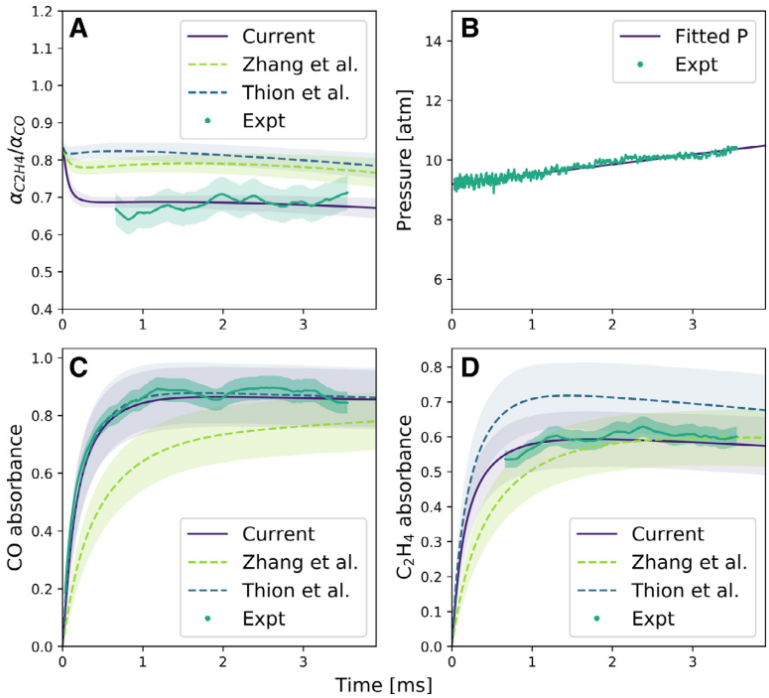

Figure 42. *Simultaneous measurements of carbon monoxide and ethylene during the pyrolysis of 0.4% cyclopentanone in argon. The ratio of C2H4/CO confirms that radical involved breakdown of cyclopentanone is an important pyrolysis pathway. This data was published as part of the Co-Optima project by Dong et al.*[25]

5.2 Validate Year 2 Models vs Experiments

In the second project year, kinetic models for butyl acetate isomers (Y2 models) were constructed and validated. To investigate the differences in reaction chemistry of BA isomers, we conducted pyrolysis experiments of four isomers of butyl acetate behind the reflected shock waves at temperatures 1296 – 1756 K and pressures of 1.2 – 1.5 atm and measured the carbon monoxide (CO) concentration-time histories using the laser absorption technique developed in Section 2.1.

A sample of these experiments is presented in Figure 43 that compares CO formation during pyrolysis of nBA, iBA, tBA, and sBA at around 1420 K and 1.4 atm. As observed, CO yields for these isomers are similar within the uncertainty.

A comparison between experimental data and model prediction over the range of measurements is shown in Figure 44. As can be seen at the temperature range of 1300 – 1550 K, the predictions have a reasonable agreement with the experimental data, showing that the model captured important pyrolysis pathways that are important for rich-condition oxidation and high-temperature ignition prediction. However, significant differences can be found at extremely high temperatures (~1700 K). The limitation of our parameters can explain the discrepancies. C-C and C-O bond fissions become more important at those temperatures but are not captured in the combustion models we developed.

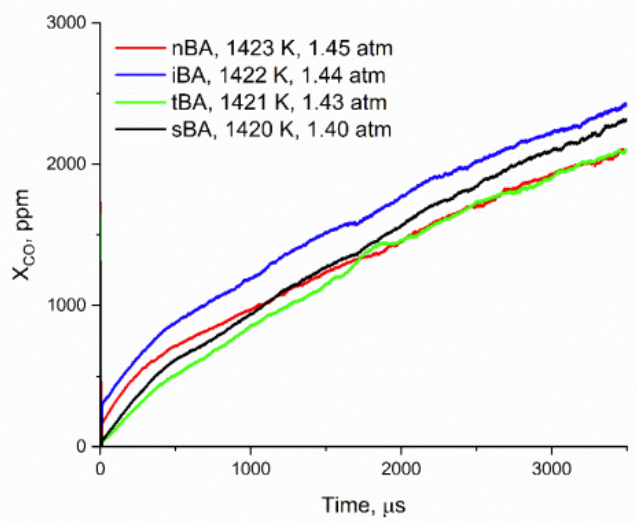

Figure 43. *CO concentration-time histories during pyrolysis of butyl acetate isomers at around 1420 K and 1.4 atm from Arafin et al.*[42]

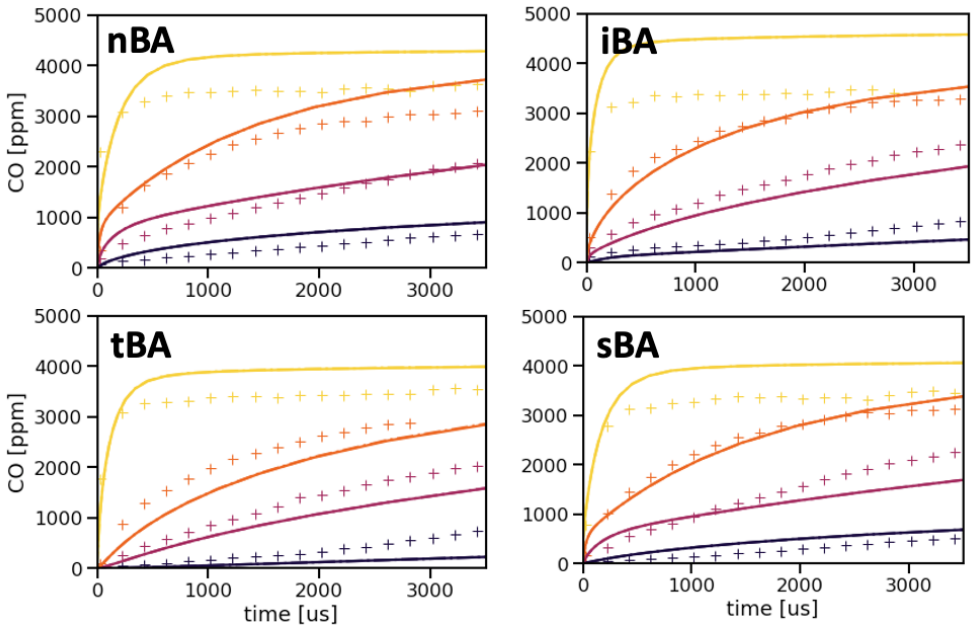

Figure 44. *Predicted and measured time histories of carbon monoxide mole fraction behind the reflected shock at various conditions. Yellow: around 1725 K, 1.3 atm; orange: around 1520 K, 1.4 atm; violet: around 1420K, 1.4 atm; black: around 1300 K 1.5 atm.*

5.3 Validate Year 3 models vs Experiments

Due to delays in the model generation (in part due to the closure of MIT for several months) and due to the laboratory closure at UCF during the COVID-19 pandemic, we were unable to experimentally validate the models that were developed in the project year 3.

Chapter 6 Time Histories of Other Species

6.1 Low P Measurements

Measurements of other hydrocarbon combustion intermediates, including methane, ethylene, carbon dioxide, and water, were also investigated. The majority of other species measurements were made using an optical parametric oscillator (OPO, scheme shown in Figure 45) which is a broadband source outputting from 3000-3500cm^{-1}. The advantage of using this optical diagnostic over fixed wavelength techniques is that the OPO is capable of deconvoluting the spectra of species with competing features, as long as strong characterizations are done beforehand. For example, the spectra of CH_4, C_2H_4, and C_2H_6 were measured in argon to map the spectrum of each molecule (Figure 46). A database for each molecule is generated over the temperature and pressure range. When the diagnostic is used in a practical fuel mixture, the measured spectra, which consists of spectra from several different intermediates, can be deconvolved through a least-squares fitting routine and the generated database. An example of this technique is shown in Figure 47, where the concentrations of CH_4, C_2H_4, and C_2H_6 were successfully measured through this technique.

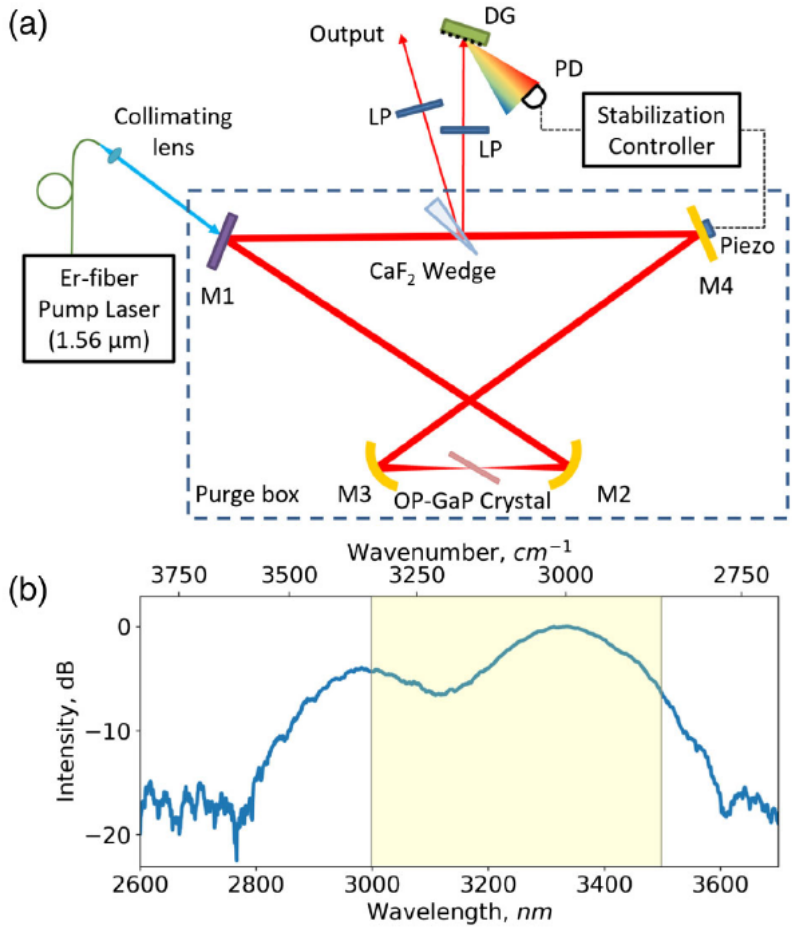

Figure 45. *(a) Schematic of the OPO. LP: long pass filter, DG: diffraction grating, PD: photodiode. M1 is a dielectric mirror transmissive to the pump and reflective for the OPO. M2 and M3 are gold coated off-axis parabolic mirrors, and M4 is a piezo-mounted flat gold mirror. (b) Stabilized output spectrum of the OPO, log scale, with the highlighted region showing the range of the time-resolved spectrometer.*

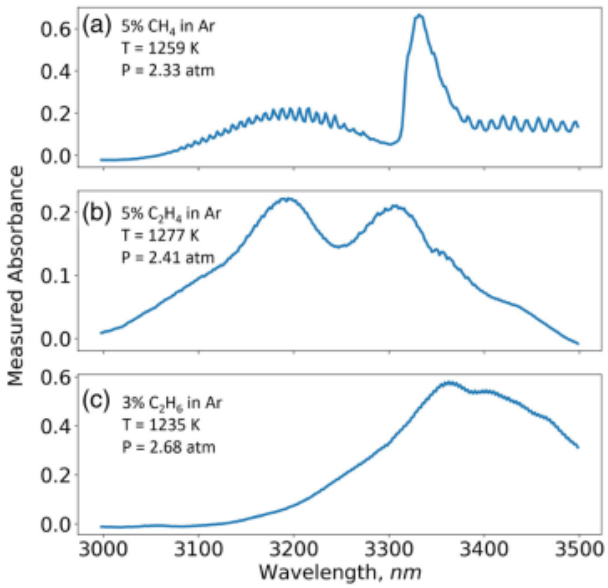

Figure 46. *Average measured absorbance spectra over the first 2 md after the reflected shock for (a) CH4 at 1259 K and 2.33 atm, (b) C2H4 at 1277 K and 2.41 atm, and (c) C2H6 at 1235 K and 2.68 atm.*

In addition to the OPO, fixed wavelength techniques were also used to measure other hydrocarbon intermediates. During the pyrolysis of cyclopentanone, we successfully measured carbon monoxide, ethylene, and cyclopentanone simultaneously (Figure 48 C, D, and E).

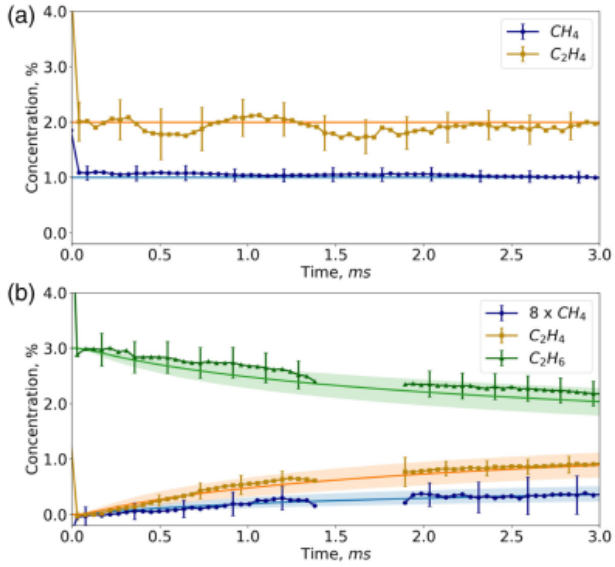

Figure 47. *Measured and expected time-histories for (a) shock heating of 1%CH_4/2%C_2H_4/Ar to 1261 K and 2.57 atm, and (b) the pyrolysis of 3%C_2H_6 in Ar at 1235 K and 2.68 atm. CH_4 scaled by 8x for visibility.*

Configured diagnostics for other species include:

- CH_4 time histories were measured using a distributed feedback interband cascade laser (ICL) centered at 3403nm from Nanoplus
- C_2H_4 time histories were measured at 10.532μm using the P14 line of a tunable CO_2 gas laser from Access Laser
- CO_2 time histories were measured using a Fabry-Perot QCL centered at 4.4μm from Thorlabs
- H_2O time histories were measured with a QCL from Nanoplus centered at 2.48 nm.

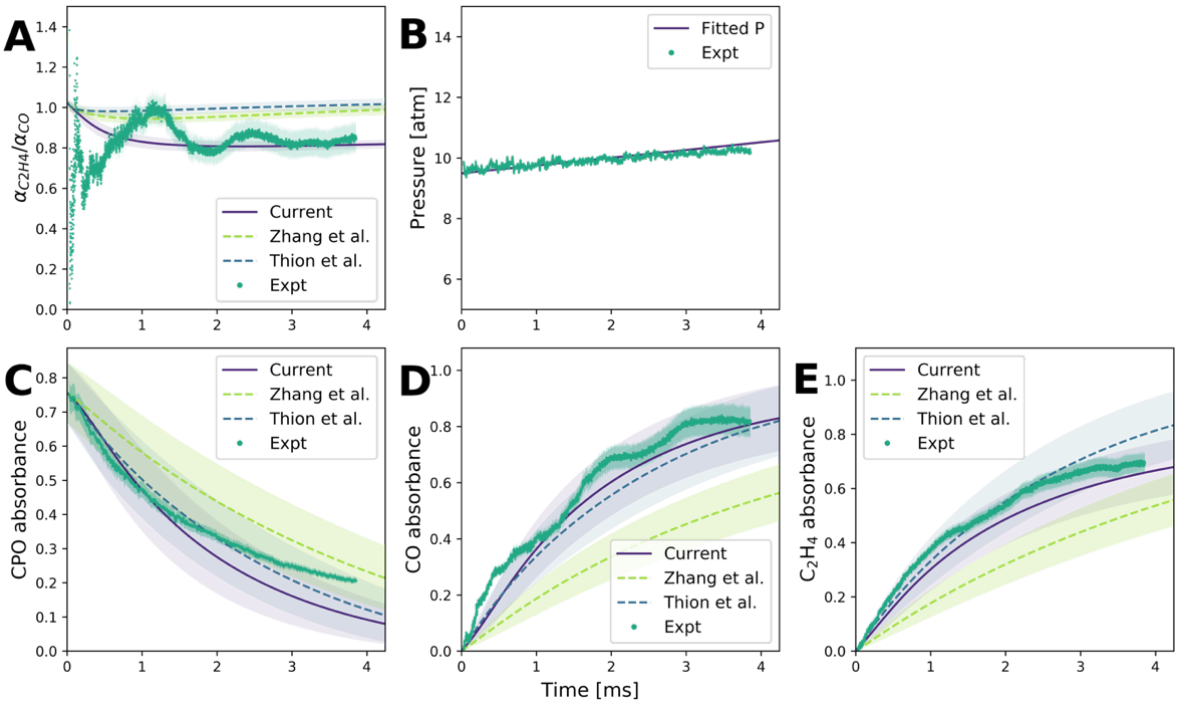

Figure 48. *Simultaneous measurements of carbon monoxide and ethylene during the pyrolysis of 0.1% cyclopentanone in argon. The ratio of C_2H_4/CO confirms that radical involved breakdown of cyclopentanone is an important pyrolysis pathway. This data was published as part of the Co-Optima project by Dong et al.*[25]

6.2 High P Measurements

We have developed techniques to measure time-resolved, *in-situ* measurements of combustion intermediates including C_2H_4, H_2O, CO_2, and CH_4, and used the developed technique C_2H_4 quantification to measure time-histories during ethanol oxidation at 20 atm with a similar experimental setup as described in Section 6.1.

Chapter 7 Method to Model Fuels with Imperfectly Known Compositions

7.1 Methodology

Biofuels can be split into two categories: (1) the fuel's composition is completely known, and (2) fuels with so many components that it is impractical with current analytical chemistry to fully characterize its composition. The previous chapters focused on fuels of known composition. For the second category fuels (Cat. 2 fuels), two different methods were explored for modeling its combustion chemistry: 1. dummy network optimization approach and sensitive-parameter optimization approach. While both approaches require model optimization to capture fuel characteristics from experimental data, the identification/proposal of the parameters to be optimized is different. In the dummy network optimization approach, a set of dummy species and their reactions were proposed and optimized (an example of a dummy network is shown in Figure 49). In the sensitive-parameter optimization approach, sensitivity analysis is used to identify reactions that will cause the largest change to the observables.

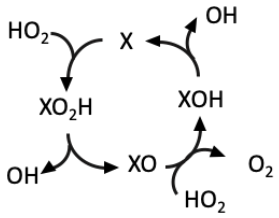

Figure 49. *A minimal dummy network with dummy species (X) and its derivatives and their reactions. For clearer illustration, arrows are chosen to be single directional, however the actual reactions are set to be reversible.*

Several scripts based on the Cantera[43] package were built, including data generation, reference curve generation, and model modification. Synthetic data of Cat 2 fuels were created based on the butanol model from Sarathy et al.[44] to test the methodology.

For dummy network optimization approach, ideally, by reasonably choosing a surrogate model, the chemistry of intermediates and chain-branching pathways will not be too different from their actual counterpart in the Cat. 2 fuel mixture networks; the dummy network can help adjust the OH generation and balance the OH/HO2 concentrations according to the actual experimental response. However, according to our quantitative test on the butanol isomer, although this approach could change the ignition delay time, the range of the change is very limited and make this method inappropriate. We observed that (1) the mole fraction ratio between OH and HO2 could be altered significantly but usually in a pattern where x_{OH} differences (within an order of magnitude) were much smaller than x_{HO2} differences, before and after the addition of dummy network; (2) a much larger OH production rate could be achieved, but it did not activate the chain branching reactions; (3) compared to the traditional model optimization, where the variables were bounded by their uncertainties, the bounds were no longer definite, and bad choices of boundaries can easily make the system stiff and difficult to converge. We then fell back to the method of the sensitive-species optimization approach.

The sensitive-species optimization approach started from a surrogate model that has similar functional groups as found in the actual Cat. 2 fuels. Then four steps were applied to the model, and its parameters were modified to allow a better match for the experimental observables:

1. Conduct sensitivity analysis at a set of extreme conditions (according to actual conditions to simulate) and select sensitive reactions with a balanced number of fundamental reactions and group-specific reactions.

2. Normalize sensitive parameters (preexponential factors of rates) and rescale the observables.

3. Generate response surface for each observable by constructing a second-order polynomial response surface and apply the sensitivity analysis based (SAB) method reported by Davis et al.[45]

4. Optimization on a root mean squared loss function composed by response surface.

7.2 Validate with Experiments

As mentioned in the other part of this report, the COVID-19 pandemic caused the closure of campus and significantly delayed our experiment schedule. Due to the limited resources and the urgency of other experiments under this project after reopening, no experimental data was generated for validating the methodology proposed for fuels with composition imperfectly known.

Chapter 8 Project Management and Reporting

Required management reporting was accomplished as scheduled.

Conclusions

The goal of this project was to develop and demonstrate a workflow for constructing chemical kinetic models for proposed biofuels, and to experimentally verify the accuracy of these computer models. The chemical kinetic models are useful for assessing the performance of a proposed biofuel (e.g., to decide if the biofuel will have desirable octane numbers, phi sensitivity, or other key metrics. These fuel performance metrics go into decisions about which biofuels are most valuable to produce.). If accurate enough the kinetic models could be useful in engine simulations, to assist in co-optimization of the engine to match the fuel. To provide a more reliable assessment of the model accuracy, we developed advanced laser probes for specific reaction intermediates, and compared their measured time-profiles with the model predictions.

Overall, the project was highly successful, leading to many improvements in the model-construction workflow, useful kinetic models for many biofuels, many of them validated, and new laser diagnostics and useful open-source software that can be used by others to create accurate models for additional biofuels. These many advances are explained/demonstrated in more than 10 journal papers plus 21 conference papers/presentations (see below for the list). However, due to the pandemic the experimental laboratories were closed, and some other portions of the work were also disrupted during the last 10 months of the project, so we were unable to complete the work mentioned in Sections 3.2, 5.3, and 7.2.

At the time this project began, it was not clear if it would be possible to accurately quantitatively predict the chemistry of new biofuels on the computer before actually manufacturing and testing them.

In this project we have demonstrated that it is indeed possible to predict biofuel chemistry accurately even before ever manufacturing or testing the biofuel. We have developed, tested, and demonstrated much of the workflow needed to make predictive modeling of biofuel chemistry into a practical and convenient engineering design tool. This research also helps lay out a path for future advances in this sub-field that would expand the range of biofuels that could be predicted, and further improve the accuracy of the predictions.

Financial Management

1. Partial salary support provided to following personnel

Senior Personnel:

MIT: William H. Green (PI)

UCF: Subith Vasu (co-PI)

Graduate students:

MIT: Xiaorui Dong, Matthew Johnson

UCF: Erik Ninnemann (lead graduate student), Farhan Arafin, Andrew Laich, Ramees Rahman, Justin Urso, Owen Pryor

Undergraduate students:

UCF: Jessica Baker, Emma Shafer

Postdocs:

MIT: Duminda Ranasinghe, Sarah Khanniche

2. Travel support provided to attend

The international combustion symposium, Dublin, Ireland, 2018 (Subith Vasu)

U.S. Combustion meeting, Pasadena, CA 2019 (Andrew Laich)

AIAA Scitech meeting 2020, Orlando, FL (Erik Ninnemann)

UTSR Meeting, 2019, Orlando, FL (Erik Ninnemann)

Clearwater Clean Energy Conference, FL, 2019 (Erik Ninnemann)

List of Publications partially or fully supported by the project

1. Ninnemann, Erik, Owen Pryor, Samuel Barak, Sneha Neupane, Zachary Loparo, Andrew Laich, and **Subith S. Vasu**. "Reflected shock-initiated ignition probed via simultaneous lateral and endwall high-speed imaging with a transparent, cylindrical test-section." ***Combustion and Flame*** 224 (2021): 43-53.
2. Hakimov, Khaiyom, Farhan Arafin, Khalid Aljohani, Khalil Djebbi, Erik Ninnemann, **Subith S. Vasu**, and Aamir Farooq. "Ignition delay time and speciation of dibutyl ether at high pressures." ***Combustion and Flame*** 223 (2021): 98-109.
3. Dong, Shijun, Kuiwen Zhang, Erik M. Ninnemann, Ahmed Najjar, Goutham Kukkadapu, Jessica Baker, Farhan Arafin, Zhandong Wang, William J. Pitz, **Subith S. Vasu**, S. Mani Sarathy, Peter K. Senecal, and Herny J. Curran. "A comprehensive experimental and kinetic modeling study of 1-and 2-pentene." ***Combustion and Flame*** 223 (2021): 166-180.
4. Johnson, Matthew S., Mark R. Nimlos, Erik Ninnemann, Andrew Laich, Gina M. Fioroni, Dongil Kang, Lintao Bu, Duminda S. Ranasinghe, Sarah Khanniche, S. Scott Goldsborough, **Subith S. Vasu**, and **William H. Green**. "Oxidation and pyrolysis of methyl propyl ether." ***International Journal of Chemical Kinetics***. 53 (2021) 915-938.
5. Arafin, Farhan, Andrew Laich, Erik Ninnemann, Robert Greene, Ramees K. Rahman, and **Subith S. Vasu**. "Influence of the double bond position in combustion chemistry of methyl butene isomers: A shock tube and laser absorption study." ***International Journal of Chemical Kinetics*** 52.11 (2020): 739-751. **Invited Special Issue.** Cover Feature Article
6. Dong, Xiaorui, Erik Ninnemann, Duminda S. Ranasinghe, Andrew Laich, Robert Greene, **Subith S. Vasu**, and **William H. Green**. "Revealing the critical role of radical-involved pathways in high temperature cyclopentanone pyrolysis." ***Combustion and Flame*** 216 (2020): 280-292.
7. Barak, Samuel, Ramees K. Rahman, Sneha Neupane, Erik Ninnemann, Farhan Arafin, Andrew Laich, Anthony C. Terracciano, and **Subith S. Vasu**. "Measuring the effectiveness of high-performance Co-Optima biofuels on suppressing soot formation at high temperature." ***Proceedings of the National Academy of Sciences (PNAS)*** 117.7 (2020): 3451-3460.
8. Laich, Andrew R., Erik Ninnemann, Sneha Neupane, Ramees Rahman, Samuel Barak, William J. Pitz, S. Scott Goldsborough, and **Subith S. Vasu**. "High-pressure shock tube study of ethanol oxidation: Ignition delay time and CO time-history measurements." ***Combustion and Flame*** 212 (2020): 486-499
9. Ninnemann, Erik, Gihun Kim, Andrew Laich, Bader Almansour, Anthony C. Terracciano, Suhyeon Park, Kyle Thurmond, Sneha Neupane, Scott Wagnon, William J Pitz, and **Subith Vasu**. "Co-optima fuels combustion: A comprehensive experimental investigation of prenol isomers." ***Fuel*** 254 (2019): 115630.
10. Khanniche, Sarah, and **William H. Green**. "Reaction Pathways, Thermodynamics, and Kinetics of Cyclopentanone Oxidation Intermediates: A Theoretical Approach." ***The Journal of Physical Chemistry A*** 123.45 (2019): 9644-9657.
11. Zhang, Kuiwen, Nitin Lokachari, Erik Ninnemann, Sarah Khanniche, **William H. Green**, Henry J. Curran, **Subith S. Vasu**, and William J. Pitz. "An experimental, theoretical, and modeling study of the ignition behavior of cyclopentanone." ***Proceedings of the Combustion Institute*** 37.1 (2019): 657-665.
12. Arafin, Farhan, Andrew Laich, Jessica Baker, Erik M. Ninnemann, and **Subith S. Vasu**. "Shock tube/laser absorption measurements of the pyrolysis of butyl acetate isomers."

AIAA Scitech 2021 Forum, Jan 11-15, 2021, virtual, paper# AIAA-2021-0988. *Peer reviewed.*

13. Dong, Xiaorui, Gianmaria Pio, Farhan Arafin, Jessica Baker, Robert Greene, Erik M. Ninnemann, **Subith S. Vasu**, and **William H. Green**. "Differences among quadruplets: A study on combustion chemistry for butyl acetate biofuel isomers" In ACS Spring 2021 National Meeting & Expo, Apr 5-16, virtual.
14. Dong, Xiaorui, Erik Ninnemann, Duminda S. Ranasinghe, Andrew Laich, Robert Greene, **Subith S. Vasu**, and **William H. Green**, "Development of a high temperature pyrolysis mechanism for cyclopentanone, a potential biofuel derived from biomass", ACS Spring 2020 National Meeting & Expo, Mar 21-25, 2020, virtual, paper presentation.
15. Ninnemann, Erik M., Emma Shafer, Jessica Baker, Farhan Arafin, and **Subith Vasu**, "Autoignition delay times measurements of linear unsaturated jet fuel compounds inside a shock tube", AIAA Scitech 2020 Forum, Jan 6-10, Orlando, FL, paper# AIAA-2020-0638. *Peer reviewed.*
16. Ninnemann, Erik M., Andrew Laich, Samuel Barak, Sneha Neupane, and **Subith Vasu**, "Shock Tube Ignition and Chemical Kinetics Studies of Advanced Liquid Biofuels for Gas Turbines", The 44th International Technical Conference on Clean Energy: The Clearwater Clean Energy Conference, Jun 16-21, 2019, Clearwater, FL, paper# 172. *Peer reviewed.*
17. Laich, Andrew, Erik Ninnemann, and **Subith Vasu**, "Shock tube and Laser Absorption Investigation of Diisobutylene- An Advanced Drop-in Biofuel", 42nd International Agency Combustion Task Leaders Meeting, Aug 23-27, 2020, virtual workshop.
18. Ninnemann, Erik, Owen Pryor, Sneha Neupane, and **Subith Vasu**, "High-Speed 3-D Imaging of Ignition in a Circular Shock Tube", The 71st Annual Meeting of the American Physical Society's Division of Fluid Dynamics (DFD), Nov 18-20, 2018, Atlanta, Georgia, vol. 63, paper# M02-05. *Peer reviewed.*
19. Arafin, Farhan, Andrew Laich, Erik Ninnemann, Robert Greene, Ramees K. Rahman, **Subith S. Vasu**, "Methyl butene isomers ignition inside a shock tube", Spring Technical Meeting, Eastern State Section Combustion Meeting, Mar 8-11, 2020, Columbia, SC, paper# 1A10.
20. Zhang, Kuiwen, Guillaume Dayma, Alexander Konnov, **Subith Vasu**, and William Pitz, "Development and validation of a chemical kinetic model for diisobutylene, a high-performance fuel", International Energy Agency Combustion Task Leaders Meeting, Jun 10-14, 2018, Fréjus, France, poster presentation.
21. Laich, Andrew, Erik M. Ninnemann, Sneha Neupane, and **Subith Vasu,** "Ignition delay time and CO time-history measurements in a shock tube during high performance jet fuel surrogate combustion", AIAA Scitech 2020 Forum, Jan 6-10, Orlando, FL, paper# AIAA-2020-2083. *Peer reviewed.*
22. Ninnemann, Erik M., Andrew Laich, Jessica Baker, Robert Greene, and **Subith Vasu,** "Time-resolved measurements of key intermediate products during cyclopentanone pyrolysis in a shock tube", AIAA Scitech 2020 Forum, Jan 6-10, Orlando, FL, paper#AIAA-2020-0767. *Peer reviewed.*
23. Arafin, Farhan, Andrew Laich, Ramees Rahman, Erik M. Ninnemann, Robert Greene, Jessica Baker, and **Subith Vasu,** "Shock tube and laser absorption study of CO time-histories during combustion of branched alkenes." AIAA Scitech 2020 Forum, Jan 6-10, Orlando, FL, paper# AIAA-2020-2146. *Peer reviewed.*
24. Johnson, Matthew S., and **William H. Green**. "Methyl propyl ether combustion." 38th Northeast Regional Meeting on Kinetics and Dynamics, Jan 25, 2020, Cambridge, MA.

25. Laich, Andrew R., Erik Ninnemann, Sneha Neupane, Kyle Thurmond, Scott Wagnon, William J. Pitz, **S.S. Vasu**, “Shock tube ignition study of prenol – a “hyperboosting” fuel relevant to the co-optima initiative”, 11th U.S. National Combustion Meeting, Mar 24-27, 2019, Pasadena, CA, paper# 2A09. *Peer reviewed.*
26. Ninnemann, Erik M., Owen Pryor, Sneha Neupane, Samuel Barak, and **Subith Vasu**, "High-speed 4-D Imaging Study of Isooctane Combustion in a Shock Tube", AIAA Scitech, Jan 7-11, 2019, San Diego, CA, paper# AIAA-2019-0119. *Peer reviewed.*
27. Laich, Andrew, Erik M. Ninnemann, Owen Pryor, Sneha Neupane, and **Subith Vasu,** "A shock tube and laser absorption study of CO time-histories during bio ether oxidation", AIAA Scitech 2019 Forum, Jan 7-11, 2019, San Diego, CA, paper# AIAA-2019-2247. *Peer reviewed.*
28. Johnson, Matthew S., and **William H. Green**. "A decision tree based machine learning algorithm for rate estimation", 2019 AIChE Annual Meeting, Nov 10-15, 2019, Orlando, FL.
29. Khanniche, Sarah, and **William H. Green**. "Reaction pathways of cyclopentanone oxidation intermediates", 11th International Conference on Chemical Kinetics, June 23-27, 2019, Orleans, France.
30. Ninnemann, Erik, Andrew Laich, Sneha Neupane, Samuel Barak, **Subith Vasu**, Owen Pryor, and Zachary Loparo. "Pyrolysis of cyclopentanone: A shock tube and laser absorption study", Joint Propulsion Conference, Jul 9-11, 2018, Cincinnati, OH, paper # 4474. *Peer reviewed.*
31. Khanniche, Sarah, Matthew S. Johnson, and **William H. Green**. "Chemical mechanism and kinetics of cyclopentanone combustion: A theoretical and RMG approach", ACS fall 2018 National Meeting & Expo, Aug 19-23, 2018, Boston, MA.
32. Khanniche, Sarah, Matthew S. Johnson, and **William H. Green**. "Fighting climate change with ab initio calculations: the example of cyclopentanone ass a promising biofuel candidate". 2018 Clean Energy Education and Empowerment (C3D) Women in Energy Symposium, Dec 3-4, 2018, Palo Alto, CA, poster presentation. *Poster competition winner.*

References

1. Gao, C. W., Allen, J. W., Green, W. H. & West, R. H., "Reaction Mechanism Generator: Automatic construction of chemical kinetic mechanisms," *Comput. Phys. Commun.* **203,** 212–225 (2016). DOI: 10.1016/j.cpc.2016.02.013
2. Hansen, N., Merchant, S. S., Harper, M. R. & Green, W. H., "The predictive capability of an automatically generated combustion chemistry mechanism: Chemical structures of premixed iso-butanol flames," *Combust. Flame* **160,** 2343–2351 (2013). DOI: 10.1016/j.combustflame.2013.05.013
3. Zhang, K., Lokachari, N., Ninnemann, E., Khanniche, S., Green, W. H., Curran, H. J., Vasu, S. S. & Pitz, W. J., "An experimental, theoretical, and modeling study of the ignition behavior of cyclopentanone," *Proc. Combust. Inst.* **37,** 657–665 (2019). DOI: 10.1016/j.proci.2018.06.097
4. Rothman, L. S., Gordon, I. E., Babikov, Y., Barbe, A., Chris Benner, D., Bernath, P. F., Birk, M., Bizzocchi, L., Boudon, V., Brown, L. R., Campargue, A., Chance, K., Cohen, E. A., Coudert, L. H., Devi, V. M., Drouin, B. J., Fayt, A., Flaud, J. M., Gamache, R. R., Harrison, J. J., Hartmann, J. M., Hill, C., Hodges, J. T., Jacquemart, D., Jolly, A., Lamouroux, J., Le Roy, R. J., Li, G., Long, D. A., Lyulin, O. M., Mackie, C. J., Massie, S. T., Mikhailenko, S., Müller, H. S. P., Naumenko, O. V., Nikitin, A. V., Orphal, J., Perevalov, V., Perrin, A., Polovtseva, E. R., Richard, C., Smith, M. A. H., Starikova, E., Sung, K., Tashkun, S., Tennyson, J., Toon, G. C., Tyuterev, V. G. & Wagner, G., "The HITRAN2012 molecular spectroscopic database," *J. Quant. Spectrosc. Radiat. Transf.* **130,** 4–50 (2013). DOI: 10.1016/j.jqsrt.2013.07.002
5. Ninnemann, E., Kim, G., Laich, A., Almansour, B., Terracciano, A. C., Park, S., Thurmond, K., Neupane, S., Wagnon, S., Pitz, W. J. & Vasu, S. S., "Co-optima fuels combustion: A comprehensive experimental investigation of prenol isomers," *Fuel* **254,** 115630 (2019). DOI: 10.1016/j.fuel.2019.115630
6. Thion, S., Togbé, C., Dayma, G., Serinyel, Z. & Dagaut, P., "Experimental and Detailed Kinetic Modeling Study of Cyclopentanone Oxidation in a Jet-Stirred Reactor at 1 and 10 atm," *Energy and Fuels* **31,** 2144–2155 (2017). DOI: 10.1021/acs.energyfuels.6b02061
7. Metcalfe, W. K., Pitz, W. J., Curran, H. J., Simmie, J. M. & Westbrook, C. K., "The development of a detailed chemical kinetic mechanism for diisobutylene and comparison to shock tube ignition times," *Proc. Combust. Inst.* **31 I,** 377–384 (2007). DOI: 10.1016/j.proci.2006.07.207
8. Hu, E., Yin, G., Gao, Z., Liu, Y., Ku, J. & Huang, Z., "Experimental and kinetic modeling study on 2,4,4-trimethyl-1-pentene ignition behind reflected shock waves," *Fuel* **195,** 97–104 (2017). DOI: 10.1016/j.fuel.2017.01.055
9. Li, H., Qiu, Y., Wu, Z., Wang, S., Lu, X. & Huang, Z., "Ignition delay of diisobutylene-containing multicomponent gasoline surrogates: Shock tube measurements and modeling study," *Fuel* **235,** 1387–1399 (2019). DOI: 10.1016/j.fuel.2018.08.132
10. Nimlos, M. R., Bu, L., Johnson, M. S., Kang, D., Fioroni, G. M., McCormick, R. L., Kim, S. A., Foust, T. D., Goldsburough, S. S. & Green, W. H., *Low Temperature Oxidation of Methylpropyl Ether* (2020).
11. Li, W., Wang, G., Li, Y., Li, T., Zhang, Y., Cao, C., Zou, J. & Law, C. K., "Experimental and kinetic modeling investigation on pyrolysis and combustion of n-butane and i-butane at various pressures," *Combust. Flame* **191,** 126–141 (2018). DOI: 10.1016/j.combustflame.2018.01.002
12. Abianeh, O. S., Oehlschlaeger, M. A. & Sung, C. J., "A surrogate mixture and kinetic mechanism for emulating the evaporation and autoignition characteristics of gasoline fuel," *Combust. Flame* **162,** 3773–3784 (2015). DOI: 10.1016/j.combustflame.2015.07.015

13. Al Rashidi, M. J., Mehl, M., Pitz, W. J., Mohamed, S. & Sarathy, S. M., "Cyclopentane combustion chemistry. Part I: Mechanism development and computational kinetics," *Combust. Flame* **183,** 358–371 (2017). DOI: 10.1016/j.combustflame.2017.05.018
14. Laich, A. R., Ninnemann, E., Neupane, S., Rahman, R., Barak, S., Pitz, W. J., Goldsborough, S. S. & Vasu, S. S., "High-pressure shock tube study of ethanol oxidation: Ignition delay time and CO time-history measurements," *Combust. Flame* **212,** 486–499 (2020). DOI: 10.1016/j.combustflame.2019.11.016
15. Zhang, Y., El-Merhubi, H., Lefort, B., Le Moyne, L., Curran, H. J. & Kéromnès, A., "Probing the low-temperature chemistry of ethanol via the addition of dimethyl ether," *Combust. Flame* **190,** 74–86 (2018). DOI: 10.1016/j.combustflame.2017.11.011
16. Metcalfe, W. K., Burke, S. M., Ahmed, S. S. & Curran, H. J., "A Hierarchical and Comparative Kinetic Modeling Study of $C_1 - C_2$ Hydrocarbon and Oxygenated Fuels," *Int. J. Chem. Kinet.* **45,** 638–675 (2013). DOI: 10.1002/kin.20802
17. Mittal, G., Burke, S. M., Davies, V. A., Parajuli, B., Metcalfe, W. K. & Curran, H. J., "Autoignition of ethanol in a rapid compression machine," *Combust. Flame* **161,** 1164–1171 (2014). DOI: 10.1016/j.combustflame.2013.11.005
18. Blowers, P. & Masel, R., "Engineering approximations for activation energies in hydrogen transfer reactions," *AIChE J.* **46,** 2041–2052 (2000). DOI: 10.1002/aic.690461015
19. Evans, M. G. & Polanyi, M., "Further considerations on the thermodynamics of chemical equilibria and reaction rates," *Trans. Faraday Soc.* **32,** 1333–1360 (1936). DOI: 10.1039/TF9363201333
20. Gao, C. W., Liu, M. & Green, W. H., "Uncertainty analysis of correlated parameters in automated reaction mechanism generation," *Int. J. Chem. Kinet.* **52,** 266–282 (2020). DOI: 10.1002/kin.21348
21. Burke, M. P., Chaos, M., Ju, Y., Dryer, F. L. & Klippenstein, S. J., "Comprehensive H 2/O 2 kinetic model for high-pressure combustion," *Int. J. Chem. Kinet.* **44,** 444–474 (2012). DOI: 10.1002/kin.20603
22. Hashemi, H., Christensen, J. M., Gersen, S., Levinsky, H., Klippenstein, S. J. & Glarborg, P., "High-pressure oxidation of methane," *Combust. Flame* **172,** 349–364 (2016). DOI: 10.1016/j.combustflame.2016.07.016
23. Curtiss, L. A., Redfern, P. C. & Raghavachari, K., "Gaussian-4 theory," *J. Chem. Phys.* **126,** 084108 (2007). DOI: 10.1063/1.2436888
24. Khanniche, S. & Green, W. H., "Reaction Pathways, Thermodynamics, and Kinetics of Cyclopentanone Oxidation Intermediates: A Theoretical Approach," *J. Phys. Chem. A* **123,** 9644–9657 (2019). DOI: 10.1021/acs.jpca.9b05806
25. Dong, X., Ninnemann, E., Ranasinghe, D. S., Laich, A., Greene, R., Vasu, S. S. & Green, W. H., "Revealing the critical role of radical-involved pathways in high temperature cyclopentanone pyrolysis," *Combust. Flame* **216,** 280–292 (2020). DOI: 10.1016/j.combustflame.2020.03.001
26. Montgomery, J. A., Frisch, M. J., Ochterski, J. W. & Petersson, G. A., "A complete basis set model chemistry. VI. Use of density functional geometries and frequencies," *J. Chem. Phys.* **110,** 2822–2827 (1999). DOI: 10.1063/1.477924
27. Montgomery, J. A., Frisch, M. J., Ochterski, J. W. & Petersson, G. A., "A complete basis set model chemistry. VII. Use of the minimum population localization method," *J. Chem. Phys.* **112,** 6532–6542 (2000). DOI: 10.1063/1.481224
28. Zhou, C.-W., Simmie, J. M., Pitz, W. J. & Curran, H. J., "Toward the Development of a Fundamentally Based Chemical Model for Cyclopentanone: High-Pressure-Limit Rate Constants for H Atom Abstraction and Fuel Radical Decomposition," *J. Phys. Chem. A* **120,** 52 (2016). DOI: 10.1021/acs.jpca.6b03994
29. Gao, C. W., Allen, J. W., Green, W. H. & West, R. H., "Reaction Mechanism Generator: Automatic construction of chemical kinetic mechanisms," *Comput. Phys. Commun.* **203,**

212–225 (2016). DOI: 10.1016/j.cpc.2016.02.013
30. Zaras, A. M., Thion, S. & Dagaut, P., "Computational kinetic study for the unimolecular decomposition of cyclopentanone," *Int. J. Chem. Kinet.* **47,** 439–446 (2015). DOI: 10.1002/kin.20921
31. Giri, B. R., Alabbad, M., Barker, J. R. & Farooq, A., "High temperature unimolecular decomposition of cyclopentanone," *Proc. Combust. Inst.* **37,** 267–273 (2019). DOI: 10.1016/j.proci.2018.05.076
32. Grinberg Dana, A., Ranasinghe, D. S., Wu, H., Grambow, C., Dong, X., Johnson, M. S., Goldman, M., Liu, M. & Green, W. H., "Automatic Rate Calculator (ARC)," (2020). at <https://github.com/ReactionMechanismGenerator/ARC>
33. Mehl, M., Pitz, W. J., Westbrook, C. K. & Curran, H. J., "Kinetic modeling of gasoline surrogate components and mixtures under engine conditions," *Proc. Combust. Inst.* **33,** 193–200 (2011). DOI: 10.1016/j.proci.2010.05.027
34. Wang, H., Dames, E., Sirjean, B., Sheen, D. A., Tangko, R., Violi, A., Lai, J. Y. W., Egolfopoulos, F. N., Davidson, D. F., Hanson, R. K. & others, "A hightemperature chemical kinetic model of n-alkane (up to n-dodecane), cyclohexane, and methyl-, ethyl-, n-propyl and n-butyl-cyclohexane oxidation at high temperatures, JetSurF version 2.0; September 19, 2010," *URL (http//melchior. usc. edu/JetSurF/JetSurF2. 0)* 17–111 (2010).
35. Zhou, C. W., Li, Y., Burke, U., Banyon, C., Somers, K. P., Ding, S., Khan, S., Hargis, J. W., Sikes, T., Mathieu, O., Petersen, E. L., AlAbbad, M., Farooq, A., Pan, Y., Zhang, Y., Huang, Z., Lopez, J., Loparo, Z., Vasu, S. S. & Curran, H. J., "An experimental and chemical kinetic modeling study of 1,3-butadiene combustion: Ignition delay time and laminar flame speed measurements," *Combust. Flame* **197,** 423–438 (2018). DOI: 10.1016/j.combustflame.2018.08.006
36. Fenard, Y., Dayma, G., Halter, F., Foucher, F., Serinyel, Z. & Dagaut, P., "Experimental and modeling study of the oxidation of 1-butene and cis -2-butene in a jet-stirred reactor and a combustion vessel," *Energy and Fuels* **29,** 1107–1118 (2015). DOI: 10.1021/ef502732c
37. Pejpichestakul, W., Ranzi, E., Pelucchi, M., Frassoldati, A., Cuoci, A., Parente, A. & Faravelli, T., "Examination of a soot model in premixed laminar flames at fuel-rich conditions," *Proc. Combust. Inst.* **37,** 1013–1021 (2019). DOI: 10.1016/j.proci.2018.06.104
38. Harper, M. R., Van Geem, K. M., Pyl, S. P., Marin, G. B. & Green, W. H., "Comprehensive reaction mechanism for n-butanol pyrolysis and combustion," *Combust. Flame* **158,** 16–41 (2011). DOI: 10.1016/j.combustflame.2010.06.002
39. Sarathy, S. M., Vranckx, S., Yasunaga, K., Mehl, M., Oßwald, P., Metcalfe, W. K., Westbrook, C. K., Pitz, W. J., Kohse-Höinghaus, K., Fernandes, R. X. & Curran, H. J., "A comprehensive chemical kinetic combustion model for the four butanol isomers," (2012). DOI: 10.1016/j.combustflame.2011.12.017
40. Kalghatgi, G. T., "Fuel anti-knock quality-part I. Engine studies," in *SAE Tech. Pap.* (2001). DOI: 10.4271/2001-01-3584
41. Thion, S., Togbé, C., Dayma, G., Serinyel, Z. & Dagaut, P., "Experimental and Detailed Kinetic Modeling Study of Cyclopentanone Oxidation in a Jet-Stirred Reactor at 1 and 10 atm," *Energy and Fuels* **31,** 2144–2155 (2017). DOI: 10.1021/acs.energyfuels.6b02061
42. Arafin, F., Baker, J., Greene, R., Ninnemann, E. M. & Vasu, S. S., "Shock tube/laser absorption measurements of the pyrolysis of butyl acetate isomers," (2021). DOI: 10.2514/6.2021-0988
43. Goodwin, D. G., Speth, R. L., Moffat, H. K. & Weber, B. W., "Cantera: An Object-oriented Software Toolkit for Chemical Kinetics, Thermodynamics, and Transport Processes," (2018). DOI: 10.5281/zenodo.1174508
44. Sarathy, S. M., Oßwald, P., Hansen, N. & Kohse-Höinghaus, K., "Alcohol combustion chemistry," *Prog. Energy Combust. Sci.* **44,** 40–102 (2014). DOI:

10.1016/j.pecs.2014.04.003
45. Davis, S. G., Mhadeshwar, A. B., Vlachos, D. G. & Wang, H., "A new approach to response surface development for detailed gas-phase and surface reaction kinetic model optimization," *Int. J. Chem. Kinet.* **36,** 94–106 (2003). DOI: 10.1002/kin.10177